

5-2010

Implementation of an Anthropomorphic Phantom for the Evaluation of Proton Therapy Treatment Procedures

Ryan L. Grant

Follow this and additional works at: https://digitalcommons.library.tmc.edu/utgsbs_dissertations



Part of the [Medical Sciences Commons](#), and the [Physics Commons](#)

Recommended Citation

Grant, Ryan L., "Implementation of an Anthropomorphic Phantom for the Evaluation of Proton Therapy Treatment Procedures" (2010). *The University of Texas MD Anderson Cancer Center UTHealth Graduate School of Biomedical Sciences Dissertations and Theses (Open Access)*. 8.
https://digitalcommons.library.tmc.edu/utgsbs_dissertations/8

This Thesis (MS) is brought to you for free and open access by the The University of Texas MD Anderson Cancer Center UTHealth Graduate School of Biomedical Sciences at DigitalCommons@TMC. It has been accepted for inclusion in The University of Texas MD Anderson Cancer Center UTHealth Graduate School of Biomedical Sciences Dissertations and Theses (Open Access) by an authorized administrator of DigitalCommons@TMC. For more information, please contact digitalcommons@library.tmc.edu.

**Implementation of an Anthropomorphic Pelvis Phantom for the
Evaluation of Proton Therapy Treatment Procedures**

By

Ryan L. Grant, B.S.

APPROVED:

Geoffrey S. Ibbott, Ph.D.
Supervisory Professor

David S. Followill, Ph.D.

X. Ronald Zhu, Ph.D.

Narayan Sahoo, Ph.D.

Susan Tucker, Ph.D.

APPROVED:

Dean, The University of Texas
Health Science Center at Houston
Graduate School of Biomedical Sciences

**Implementation of an Anthropomorphic Pelvis Phantom for the Evaluation of
Proton Therapy Treatment Procedures**

A

THESIS

Presented to the Faculty of
The University of Texas
Health Science Center at Houston
and
The University of Texas
M. D. Anderson Cancer Center
Graduate School of Biomedical Sciences
In Partial Fulfillment

Of the Requirements

For the Degree of

MASTER OF SCIENCE

By

Ryan L. Grant, B.S.
Houston, Texas

May, 2010

Dedication

To my dad

For always reminding me

Physics is what physicists do on nights and weekends

To my mom

For always reminding me

There is food in the fridge

Acknowledgements

I would like to thank my advisor, Dr. Geoffrey Ibbott, for his guidance, support and patience throughout this project. I would also like to thank the other members of my supervisory committee: David Followill, Ron Zhu, Narayan Sahoo and Susan Tucker for their time and assistance. The people at the RPC have been a great help to me with this project and others. The built-in support system in this department has also helped me to keep my sanity and move forward every time I needed some help.

I would also like to thank the people at the Proton Therapy Center – Houston for the large amount of access to the facility. Beverly Riley provided a great amount of dosimetry support without which I would have been lost. A special thanks needs to be given to Narayan Sahoo and Michael Gillin for running the beam for 95% of my experiments. And as my experiments were late at night or Saturday morning, this time was invaluable.

Lastly, I would like to thank my friends and family for their love and support throughout the last few years. “The Good Guys” and “Team Rockstar” were the best classmates I could have asked for. My friends always seemed to know just when I needed them and my family has managed to never once threaten to disown me. Thank you.

Implementation of an Anthropomorphic Pelvis Phantom for the Evaluation of Proton Therapy Treatment Procedures

Publication No. _____

Ryan L. Grant, B.S.

Supervisory Professor: Geoffrey S. Ibbott, Ph.D.

With an increasing number of institutions offering proton therapy, the number of multi-institutional clinical trials involving proton therapy will also increase in the coming years. The Radiological Physics Center monitors sites involved in clinical trials through the use of site visits and remote auditing with thermoluminescent dosimeters (TLD) and mailable anthropomorphic phantoms. Currently, there are no heterogeneous phantoms that have been commissioned to evaluate proton therapy. It was hypothesized that an anthropomorphic pelvis phantom can be designed to audit treatment procedures (patient simulation, treatment planning and treatment delivery) at proton facilities to confirm agreement between the measured dose and calculated dose within 5%/3mm with a reproducibility of 3%. A pelvis phantom originally designed for use with photon treatments was retrofitted for use in proton therapy. The relative stopping power (SP) of each phantom material was measured. Hounsfield Units (HU) for each phantom material were measured with a CT scanner and compared to the relative stopping power calibration curve. The tissue equivalency for each material was calculated. Two proton treatment plans were created; one which did not correct for material SP differences (Plan 1) and one plan which did correct for SP differences (Plan 2). Film and TLD were loaded

into the phantom and the phantom was irradiated 3 times per plan. The measured values were compared to the HU-SP calibration curve and it was found that the stopping powers for the materials could be underestimated by 5-10%. Plan 1 passed the criteria for the TLD and film margins with reproducibility under 3% between the 3 trials. Plan 2 failed because the right-left film dose profile average displacement was -9.0 mm on the left side and 6.0 mm on the right side. Plan 2 was intended to improve the agreements and instead introduced large displacements along the path of the beam. Plan 2 more closely represented the actual phantom composition with corrected stopping powers and should have shown an agreement between the measured and calculated dose within 5%/3mm. The hypothesis was rejected and the pelvis phantom was found to be not suitable to evaluate proton therapy treatment procedures.

Table of Contents

Signature Page	i
Title Page	ii
Dedication	iii
Acknowledgements	iv
Abstract	v
Table of Contents	vii
List of Figures	x
List of Tables	xiii
Chapter 1 Introduction and Background	1
1.1 Statement of Problem	1
1.2 Proton Therapy	2
1.2.1 History	2
1.2.2 Physical Properties of Protons	3
1.2.3 Relative Biological Effectiveness	5
1.2.4 Proton Range	6
1.2.5 Beam Modification	7
1.3 Pelvis Phantom	12
1.3.1 Phantom Design	12
1.3.2 Phantom Use in Credentialing	17
1.4 Hypothesis and Specific Aims	17
Chapter 2 Materials and Methods	19

2.1	Phantom Material Stopping Powers.....	19
2.1.1	<i>Depth Dose Scanning Procedure</i>	19
2.1.2	<i>Relative Stopping Power Analysis</i>	21
2.1.3	<i>Relative Stopping Power Comparison</i>	22
2.2	Treatment Planning	22
2.2.1	<i>Treatment Plan 1</i>	24
2.2.2	<i>Treatment Plan 2 - New SP Plan</i>	26
2.3	Dosimeters	27
2.3.2	<i>Thermoluminescent Dosimeters</i>	29
2.4	Treatment Delivery	32
2.4.1	<i>Monitor Unit Calculation</i>	33
2.5	Dosimetry Data Analysis	34
2.5.1	<i>TLD Registration</i>	34
2.5.2	<i>Film Dosimetry</i>	35
2.5.3	<i>Film Registration</i>	36
2.6	Treatment Procedure Evaluation.....	37
2.6.1	<i>TLD Comparison</i>	37
2.6.2	<i>Beam Profiles Comparison</i>	38
2.6.3	<i>Treatment Plan 2 Quality Assurance</i>	38
Chapter 3	Results and Discussion.....	40
3.1	Phantom Material Stopping Powers.....	40
3.1.1	<i>Relative Stopping Power Analysis</i>	40
3.1.2	<i>Stopping Power Comparison</i>	41

3.2	Treatment Planning	43
3.2.1	<i>Treatment Plan 1</i>	43
3.2.2	<i>Treatment Plan 2 – New SP Plan</i>	43
3.3	Treatment Delivery	45
3.4	Dosimetry Data Analysis	46
3.4.1	<i>Thermoluminescent Dosimeters</i>	46
3.4.2	<i>TLD Registration</i>	47
3.4.3	<i>Film Dosimetry</i>	49
3.4.4	<i>Film Registration</i>	51
3.5	Treatment Procedure Evaluation.....	52
3.5.1	<i>TLD Comparison</i>	52
3.5.2	<i>Dose Profile Comparison</i>	57
3.5.3	<i>Treatment Plan 2 Quality Assurance</i>	67
Chapter 4	Conclusions	70
4.1	Summary	70
4.2	Conclusions.....	71
4.3	Future works	72
Chapter 5	Appendix	74
References	87
Vita	90

List of Figures

Figure 1.1: Comparisons of Depth Dose Distributions.....	3
Figure 1.2: Schematic of Nozzle Components	8
Figure 1.3: Range Modulation Wheel.....	10
Figure 1.4: Circular Aperture.....	11
Figure 1.5: Compensator.....	12
Figure 1.6: Side view Pelvis Phantom	13
Figure 1.7: Inferior view Pelvis Phantom	14
Figure 1.8: Pelvis Phantom Imaging Insert.....	14
Figure 1.9: Axial CT Slice of Pelvis Phantom.....	15
Figure 1.10: Pelvis Phantom Dosimetry Insert.....	16
Figure 2.1: Stopping Power Measurement Setup	21
Figure 2.2: Screen capture from TPS.....	24
Figure 2.3: Configuration of the Gafchromic® EBT Film	28
Figure 2.4: Dosimetry Insert.....	29
Figure 2.5: Phantom Treatment Setup	32
Figure 3.1: Depth Dose Curve with and without Nylon	40
Figure 3.2: Comparison of Relative Stopping Powers	42
Figure 3.3: Revised SP Calibration Curve.....	44
Figure 3.4: Treatment Plan Registration.....	48
Figure 3.5: Film Calibration Curve.....	50
Figure 3.6: Film Registration Points.....	52
Figure 3.7: Plan 1 Trial 1 Right-Left Profile – Coronal Plane.....	57

Figure 3.8: Plan 1 Trial 1 Superior-Inferior Profile – Coronal Plane	58
Figure 3.9: Plan 1 Trial 1 Superior-Inferior Profile – Sagittal Plane.....	59
Figure 3.10: Plan 1 Trial 1 Anterior-Posterior Profile – Sagittal Plane.....	60
Figure 3.11: Plan 2 Trial 1 Right Left Profile – Coronal Plane.....	61
Figure 3.12: Plan 2 Trial 1 Superior-Inferior Profile – Coronal Plane	62
Figure 3.13: Plan 2 Trial 1 Superior-Inferior Profile – Sagittal Plane.....	63
Figure 3.14: Plan 2 Trial 1 Anterior-Posterior Profile – Sagittal Plane.....	63
Figure 3.15: Plan 2 Verification Trial 1 Right Left Profile – Coronal Plane.....	64
Figure 3.16: Plan 2 Verification Trial 1 Superior-Inferior Profile – Coronal Plane.....	65
Figure 3.17: Plan 2 Verification Trial 1 Superior-Inferior Profile – Sagittal Plane	66
Figure 3.18: Plan 2 Verification Trial 1 Anterior-Posterior Profile – Sagittal Plane	66
Figure 3.19: Right Lateral QA Comparison	67
Figure 3.20: Left Lateral QA Comparison.....	68
Figure 5.1: Plan 1 Trial 2 Right-Left Profile – Coronal Plane.....	74
Figure 5.2: Plan 1 Trial 2 Superior-Inferior Profile – Coronal Plane	75
Figure 5.3: Plan 1 Trial 2 Superior-Inferior Profile – Sagittal Plane.....	75
Figure 5.4: Plan 1 Trial 2 Anterior-Posterior Profile – Sagittal Plane.....	76
Figure 5.5: Plan 1 Trial 3 Right-Left Profile – Coronal Plane.....	76
Figure 5.6: Plan 1 Trial 3 Superior-Inferior Profile – Coronal Plane	77
Figure 5.7: Plan 1 Trial 3 Superior-Inferior Profile – Sagittal Plane.....	77
Figure 5.8: Plan 1 Trial 3 Anterior-Posterior Profile – Sagittal Plane.....	78
Figure 5.9: Plan 2 Trial 2 Right Left Profile – Coronal Plane.....	78
Figure 5.10: Plan 2 Trial 2 Superior-Inferior Profile – Coronal Plane	79

Figure 5.11: Plan 2 Trial 2 Superior-Inferior Profile – Sagittal Plane.....	79
Figure 5.12: Plan 2 Trial 2 Anterior-Posterior Profile – Sagittal Plane.....	80
Figure 5.13: Plan 2 Trial 3 Right Left Profile – Coronal Plane.....	80
Figure 5.14: Plan 2 Trial 3 Superior-Inferior Profile – Coronal Plane	81
Figure 5.15: Plan 2 Trial 3 Superior-Inferior Profile – Sagittal Plane.....	81
Figure 5.16: Plan 2 Trial 3 Anterior-Posterior Profile – Sagittal Plane.....	82
Figure 5.17: Plan 2 Verification Trial 2 Right Left Profile – Coronal Plane.....	82
Figure 5.18: Plan 2 Verification Trial 2 Superior-Inferior Profile – Coronal Plane.....	83
Figure 5.19: Plan 2 Verification Trial 2 Superior-Inferior Profile – Sagittal Plane	83
Figure 5.20: Plan 2 Verification Trial 2 Anterior-Posterior Profile – Sagittal Plane	84
Figure 5.21: Plan 2 Verification Trial 3 Right Left Profile – Coronal Plane.....	84
Figure 5.22: Plan 2 Verification Trial 3 Superior-Inferior Profile – Coronal Plane.....	85
Figure 5.23: Plan 2 Verification Trial 3 Superior-Inferior Profile – Sagittal Plane	85
Figure 5.24: Plan 2 Verification Trial 3 Anterior-Posterior Profile – Sagittal Plane	86

List of Tables

Table 1.1: Phantom Materials Comparison with CT Values	16
Table 2.1: Beam Parameters for Treatment Plan 1	25
Table 2.2: Beam Parameters for Treatment Plan 2 – New SP Plan.....	27
Table 2.3: Dosimetry Reference Conditions.....	34
Table 3.1: Relative Stopping Powers.....	41
Table 3.2: Calculated Dose Points Plan 1	43
Table 3.3: Plan 2 CT Values	44
Table 3.4: Calculated Dose Points Plan 2	45
Table 3.5: Monitor Unit Calculation.....	46
Table 3.6: Fading Correction Constants	47
Table 3.7: 3D Coordinate Registration	48
Table 3.8: 2D Film Registration	51
Table 3.9: TLD Data from Treatment Plan 1	53
Table 3.10: TLD Data from Treatment Plan 2.....	55
Table 3.11: Average Dose Across 3 Trials	56

Chapter 1

Introduction and Background

1.1 Statement of Problem

Proton therapy is quickly expanding in the United States, with new centers offering this course of treatment opening nearly every year. The motivation for proton therapy is its ability to deliver superior dose distributions when compared to the photon treatment alternative. It has been suggested that this will allow for a more conformal treatment plan in certain disease sites and the opportunity to escalate the dose to the tumor site without increasing dose to the surrounding normal tissues (Smith 2006). For this reason, along with the availability of medical insurance reimbursement and more affordable proton producing devices (including compact cyclotrons) the production of proton therapy facilities is increasing in the United States (Smith 2009). With an increasing number of institutions offering proton therapy, the number of multi-institutional clinical trials involving proton therapy will also increase in the coming years.

The National Cancer Institute (NCI) sponsors clinical trials which are opened to participation at multiple institutions in the country. This allows for a larger number of patients to be enrolled in the different protocols. The mission of the Radiological Physics Center (RPC) is to assure the NCI and cooperative groups that the institutions participating in these clinical trials are delivering comparable and consistent doses of radiation (Followill *et al.* 2007). The RPC is able to monitor sites involved in clinical trials through the use of site visits and remote auditing with TLD and mailable heterogeneous phantoms. Currently, there are no heterogeneous phantoms that have been commissioned to evaluate proton therapy. The RPC does have a pelvis phantom which is

used to evaluate intensity-modulated radiation therapy (IMRT). The purpose of this study is to investigate the use of the current pelvis phantom for the evaluation of the treatment procedures at facilities using proton therapy.

1.2 Proton Therapy

1.2.1 History

Proton therapy is a specialized radiation therapy using charged particles (protons) to treat tumors. Robert Wilson first hypothesized that the physical properties of protons could be therapeutically advantageous (Wilson 1946). In Wilson's paper, he described how protons would traverse through the tissue in a nearly straight trajectory and deposit the majority of their dose near the distal end of their range. He also described a device which modulates the high dose at the end of the range to spread a uniform dose over a specified target volume. The first patient treatment in the US using high energy protons occurred at the University of California, Berkeley in 1954, only 8 years after Robert Wilson published his paper (Wilson 1946). The patients were treated with high-dose proton therapy to the pituitary following experiments involving mice and rats (Lawrence 1957); (Tobias *et al.* 1958). The Harvard University Cyclotron Laboratory began treating patients in 1961 for intracranial cancer due to advantages over full-penetration methods. Noted among the reasons were the increased points of possible beam entry since the characteristics of protons allowed for the avoidance of radio-sensitive structures such as the eyes (Kjellberg *et al.* 1962).

Modern proton therapy in the US began in 1990 at the Loma Linda University Medical Center (LLUMC) (Slater *et al.* 1992). This was also the first hospital-based proton facility in the United States designed specifically for medical treatments. All

previous US facilities began as research machines. The first treatment was an ocular melanoma which was followed by brain tumors and other anatomical sites with the year (Slater *et al.* 1992).

1.2.2 Physical Properties of Protons

Proton therapy is an exceptional form of radiation therapy due to its range and depth dose distribution properties. The dose from protons demonstrates a relatively uniform plateau region followed by a peak of maximum deposition at the end of the range.

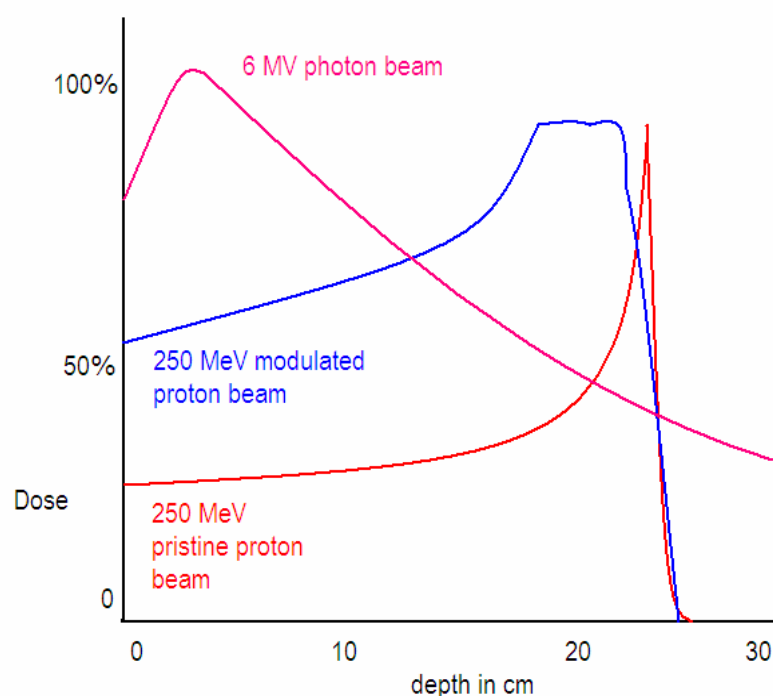


Figure 1.1: Comparisons of Depth Dose Distributions

Figure 1.1 is a comparison of the depth distributions for a 6 MV photon beam, a pristine 250 MeV proton beam and a modulated 250 MeV proton beam. The entrance

dose for the pristine proton beam is less than that of the photon beam and both proton beams have a finite range near the 26 cm mark. The photon beam continues past the end of the graph in what is called an exit dose. The region before the 100% dose region for the proton beam is called the plateau region. For the modulated proton beam, the dose in the plateau region is higher than the pristine beam. This is due to the modulation techniques of the pristine Bragg peak which is discussed in more detail in Section 1.2.5. The flat dose region at 100% of the dose in the modulated proton beam is the Spread Out Bragg Peak (SOBP). With the proton distributions, the dose then falls off to zero very rapidly which gives no dose past the region which receives the highest dose. When carefully planned, a tumor can be fully irradiated with no exit dose.

Protons are positively charged particles with a mass 1836 times that of an electron. The energy loss properties of protons allow for prediction of the range of protons in matter which is dependent on the initial energy of the protons and the density of the materials in the path of the beam. The stopping power describes the energy loss of protons due to interactions in matter.

Equation 1.1 is the formula for the mass collision stopping power from the Bethe theory which is outlined in ICRU Report 49 (ICRU 1993).

$$(1/\rho)S_{\text{col}} = -(1/\rho)(dE/dx)_{\text{el}} = \frac{4\pi r_e^2 mc^2}{\beta^2} \frac{1}{u} \frac{Z}{A} z^2 L(\beta) \quad \text{Equation 1.1}$$

For this equation, r_e is the classical electron radius, mc^2 is the electron rest energy, β is the velocity of the particle, u is the atomic mass unit, Z is the atomic number of the target atom, A is the atomic mass of the target, z is the charge number of the projectile while $L(\beta)$ is the stopping number. The stopping number depends on three factors:

1. The mean excitation energy of the medium, which quantifies the electron binding

energy. The mean excitation energies are usually obtained from experimental data.

2. The shell correction accounts for the lessening contribution from the interactions with electrons to the stopping power as the projectile velocity decreases.
3. The density-effect correction acknowledges that the passage of the projectile polarizes the medium in which the projectile is travelling. The stopping power reduces due to this polarization (ICRU 1993).

The linear energy transfer (LET) of a particle describes how the energy of the beam transfers to the irradiated material per unit particle path length (ICRU 2007). The LET can be considered a “restricted” stopping power as it does not include secondary collisions which result from the scattering of the particles. The LET for charged particles increases at the end of the track which creates what is known as the Bragg peak.

1.2.3 Relative Biological Effectiveness

The Relative Biological Effectiveness (RBE) describes the amount of dose from a radiation source needed to produce the same biological effect as a standard source of radiation and is described in Equation 1.2 (Johns and Cunningham 1983).

$$\text{RBE} = \frac{\text{Dose from standard source to produce biological effect}}{\text{Dose from test source to produce biological effect}} \quad \text{Equation 1.2}$$

For proton therapy, ICRU Report 78 recommends to use a generic RBE value of 1.1 in the clinical setting based on in-vivo laboratory studies. Along the plateau and the SOBP, the RBE does not show much variation until the distal end of the SOBP. At this location, the RBE might increase from 5-10% which can extend the biologically effective range of the beam by 1-2 mm (ICRU 2007).

Many institutions use the nomenclature “cobalt-gray equivalent” or CGE to report the equivalent dose of protons as compared to therapies with an RBE value of unity. This practice is not considered an SI unit and as such the recommended nomenclature is to use the RBE-weighted absorbed dose which is represented by D_{RBE} (seen in Equation 1.3) where D is the proton absorbed dose (in Gy) (ICRU 2007).

$$D_{\text{RBE}} = 1.1 \times D \quad \textbf{Equation 1.3}$$

In order to distinguish between D and D_{RBE} , when recording dose levels the notations of “Gy” and “Gy_{RBE}” will be used. For example, to describe the dose to the TLD in the pelvis phantom it will be denoted the TLD was irradiated to 6 Gy or to 6.6 Gy_{RBE}.

1.2.4 Proton Range

The path length of protons is determined by the energy loss of the protons as they traverse through the target material. This can be determined based on the initial energy of the proton and the material present in the path of the beam. As the beam passes through material, energy is lost due to a scattering event. Since each individual particle does not lose the same amount of energy with each interaction, the individual path lengths of each particle will differ slightly. This is called range straggling and can introduce a range uncertainty of about 1% (Breuer and Smit 2000). Along with the uncertainty of the initial energy of the beam as it leaves the nozzle (~1%) and the uncertainty attributed to the beam passing through inhomogeneities in the beam path the total range uncertainty can be on the order of 2-3% (Breuer and Smit 2000). During treatment planning for a tumor

site, this uncertainty must be taken into account to ensure the entire primary target volume (PTV) is covered.

The lateral penumbra of a proton beam is initially very sharp due to the relatively low amount of side-scatter when compared to more conventional radiotherapies. As protons penetrate through a target, the protons spread laterally primarily due to scattering. The range of the secondary electrons is typically on the order of 0.1 cm in organic material (Breuer and Smit 2000). The sharp lateral penumbra of high energy beams at shallow depths provides separation between the high dose target and the low dose normal tissues and can serve as a deciding factor for the use of proton therapy when treating near critical structures (Moyers 1999).

1.2.5 Beam Modification

As the proton beam enters the nozzle, several modifications are made to enable the use of the beam for treatment. In a passive beam, a single- or double-scattering technique can be used. A diagram showing the nozzle components for the passively scattered beam lines at the Proton Therapy center in Houston is shown in Figure 1.2 (Sahoo *et al.* 2008).

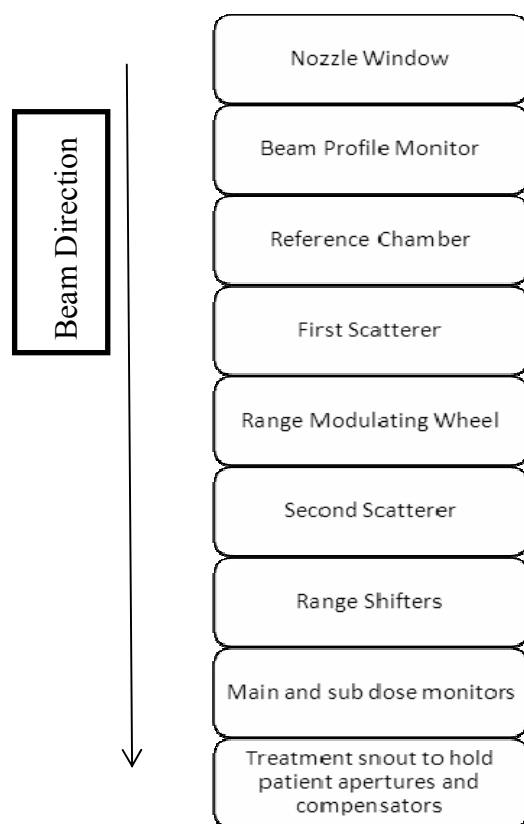


Figure 1.2: Schematic of Nozzle Components

Scattering the beam broadens the beam laterally to provide coverage across the treatment field. Protons exiting the first scatterer will have a Gaussian shaped intensity profile. As this is a non-uniform beam, a second scatterer placed downstream from the first is shaped to correct this Gaussian profile in order to create a uniform range across the axis of the beam. The lateral penumbra of the beam will broaden due to the increased amount of scatter in the beam path and should be reduced as much as possible to protect surrounding critical structures.

A pristine Bragg peak is not large enough to adequately cover a tumor site. The Bragg peak must be modulated in order to produce what is called a Spread Out Bragg Peak (SOBP). The summation of many pristine distributions consisting of various

energies will produce an extended uniform Bragg peak. The SOBP will ensure the beam covers the depth of the tumor longitudinally.

There are two main ways to position the Bragg peak within a patient. One way is to change the energy of the beam. This will accelerate or decelerate the protons allowing for the range to increase or decrease accordingly. The other way to position the Bragg peak is to introduce material in the beam path upstream from the patient. This will degrade the energy of the protons before they enter the patient and shorten the depth of beam penetration in the patient. Introducing material in the beam path is the most common way the Bragg peak is influenced in a clinical setting. The range shifter is comprised of slabs of materials with known water equivalent thicknesses (WET) that are placed downstream from the second scatterer and upstream from the patient apertures and compensators. These shifters enable the operator to move the distal end of the SOBP towards the nozzle dependent on the amount of water equivalent material placed upstream of the target.

The range modulation wheel (RMW) is a device first described by Robert Wilson and expanded upon by Koehler et al (Wilson 1946; Koehler *et al.* 1975). The RMW is a device which has staircases of materials that form two to three peaks (depending on the design of the wheel) which is programmed to spin quickly. An example of a RMW is shown in Figure 1.3.



Figure 1.3: Range Modulation Wheel

By controlling the location on the wheel where the beam starts and stops, the depths at which pristine Bragg peaks are located can be influenced. The summation of the multiple Bragg peaks creates the SOBP.

Once the energy and SOBP for the treatment have been selected, patient specific apertures and compensators are constructed according to the treatment plan. The brass apertures (Figure 1.4) collimate the beam to conform to the treatment field.



Figure 1.4: Circular Aperture

The collimation of the proton field by the patient specific apertures should be placed as close to the patient as possible due to multiple coulombic scattering in the air and the compensator as well as the projection of the effective source size (Moyers 1999). For this reason, the snout at the end of the nozzle is able to extend to be closer to the patient surface.

After the apertures, a compensator (seen in Figure 1.5) is placed on the snout to distribute the dose deposition according to the treatment plan.

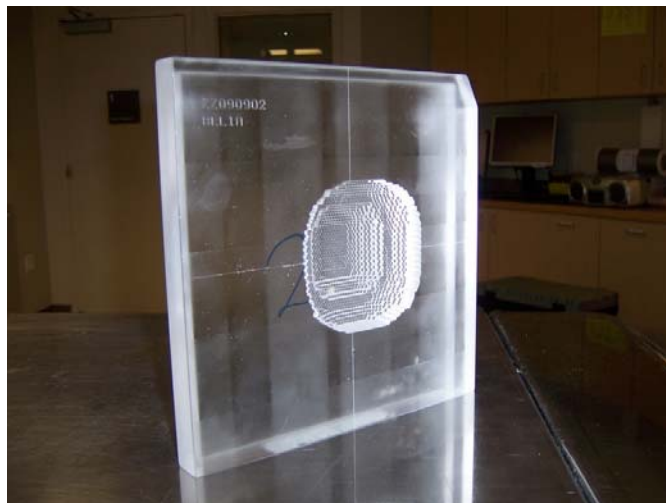


Figure 1.5: Compensator

The compensator design matches the distal edge of the SOBP to the distal side of the target, and corrects for heterogeneities in the patient and uncertainties in patient positioning (Moyers 1999).

1.3 Pelvis Phantom

The RPC has several anthropomorphic phantoms which are used as part of the credentialing services for participation in NCI sponsored clinical trials. The pelvis phantom was originally designed to be a mailable quality assurance phantom to test intensity-modulated radiation therapy (IMRT) procedures. With this in mind, the design and materials were chosen to simulate the pelvis region of a patient with anatomy present to create restrictions for the treatment planning and delivery in typical IMRT cases.

1.3.1 Phantom Design

The pelvis phantom was originally designed to be a remote auditing tool for institutions utilizing IMRT treatment plans in protocols. The phantom needed to be anatomically relevant with materials that were photon equivalent, durable enough to withstand constant shipping and also light weight to keep shipping costs at a reasonable

rate. The solution was to have a phantom that would be filled with water upon arrival at an institution. The phantom can be seen in Figure 1.6 and Figure 1.7. The green and blue knobs seen in both figures hold thermoluminescent dosimeter (TLD) capsules (Quantaflux, LLC, Dayton Ohio) in each femoral head while the other two knobs are the openings to fill and drain the water. The white region in the center is the front face of the dosimetry insert.

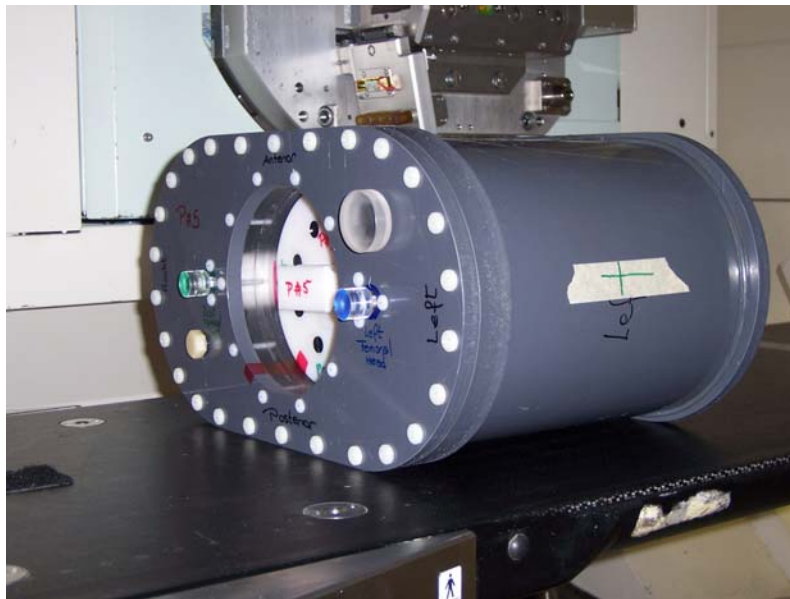


Figure 1.6: Side view Pelvis Phantom



Figure 1.7: Inferior view Pelvis Phantom

The phantom has two removable inserts: an imaging insert and a dosimetry insert. The imaging insert (seen in Figure 1.8) is a hollow shell which holds two spheres representing the bladder and prostate (also known as the “target” for this phantom) as well as a cylinder which represents the rectum. The femoral heads are located within the shell of the patient.

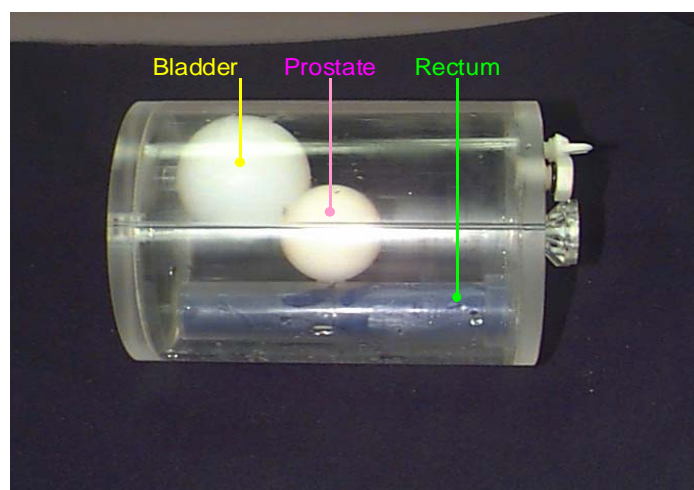


Figure 1.8: Pelvis Phantom Imaging Insert

Figure 1.9 is an axial slice of the phantom containing the imaging insert that is intended for use with treatment planning. The locations where the film and TLD are placed during treatment delivery are overlaid onto the image, but are not seen during CT simulation or treatment planning.

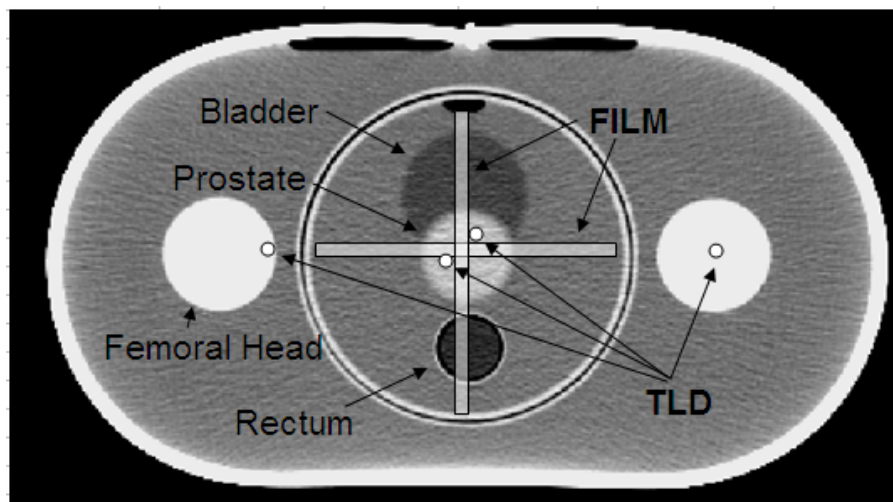


Figure 1.9: Axial CT Slice of Pelvis Phantom

The phantom materials were chosen for their equivalency based upon electron density and are shown in Table 1.1 (Radford 2001).

Material	Material Density	Material CT Number	Patient CT Number
Nylon - Prostate	1.15	1088	1026
PVC - Shell	1.37	1760	----
PBT - Bone	1.31	1203	1297
HI Polystyrene - Dosimetry Insert	1.20	974	----
Polyethylene - Bladder	0.95	923	1001
Acrylic - Bone Marrow	1.17	1123	----
Wax - Rectum	1.00	950	922

Table 1.1: Phantom Materials Comparison with CT Values

Once the treatment plan was completed, the dosimetry insert (shown in Figure 1.10) replaced the imaging insert.

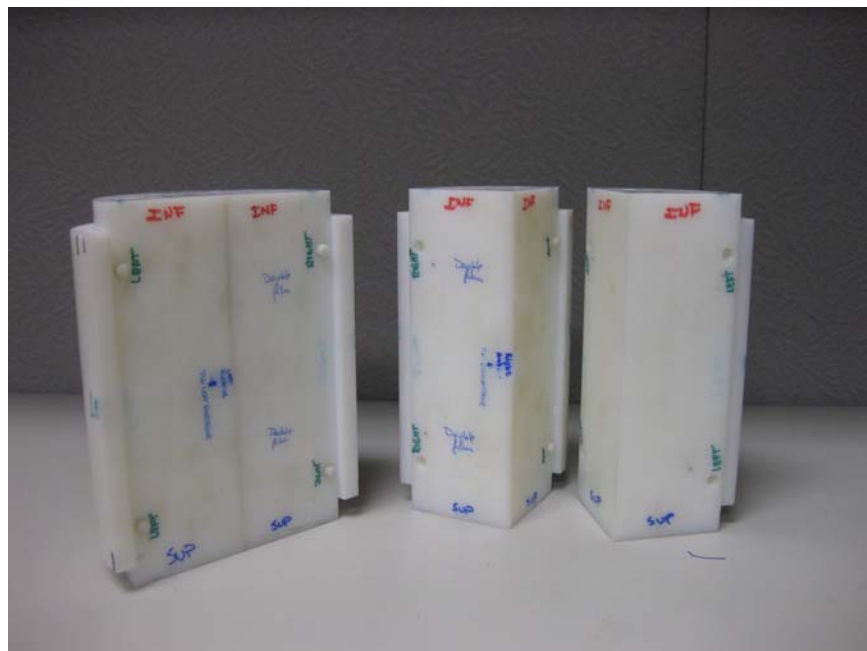


Figure 1.10: Pelvis Phantom Dosimetry Insert

This solid insert holds two TLD capsules and two pieces of radiochromic film in the orientation displayed in Figure 1.9. Two more TLD capsules are placed in the femoral

heads prior to irradiation. Solid acrylic rods are used during CT simulation.

1.3.2 Phantom Use in Credentialing

The phantoms used by the RPC are intended to measure the quality of the overall treatment procedure for institutions participating in clinical trials. Quality assurance for dose calculation and treatment verification can be difficult for advanced treatment procedures. Proton therapy dose calculations are dependent on accurate simulations and precise treatment setup to correctly deliver the intended treatment. Having a phantom which mimics patient anatomy challenges the treatment planning process and requires a realistic dose calculation for a patient treatment. Using the same phantom from treatment planning for treatment delivery tests the institution's procedures for re-creating the patient setup from the initial CT scan. This phantom should audit the accuracy of the CT simulation, challenge the treatment planning system and provide dose measurements for treatment delivery.

1.4 Hypothesis and Specific Aims

An anthropomorphic pelvis phantom can be designed to audit treatment procedures (patient simulation, treatment planning and treatment delivery) at proton facilities to confirm agreement between the measured dose and calculated dose within 5%/3mm with a reproducibility of 3%.

The hypothesis was tested through the completion of the specific aims listed below. The phantom was simulated, planned and treated to emulate a prostate treatment with proton therapy. Modifications were made throughout the process and the specific aims were reapplied as the phantom was evaluated using the agreements listed in the hypothesis. The specific aims were:

- 1) Determine the equivalency of phantom materials to their patient anatomy counterparts.
- 2) Image the pelvis phantom, create a clinically relevant treatment plan, and irradiate the phantom with this treatment plan.
- 3) Measure the delivered dose distribution and the dose to specific points within the irradiated pelvis phantom.
- 4) Compare the calculated and measured doses and dose distributions to determine the deviations and reproducibility.

Chapter 2

Materials and Methods

2.1 Phantom Material Stopping Powers

The range of protons is determined by the initial energy of the proton beam and the materials placed in the path of the beam. The relative stopping power and width of each piece of material in the path of the beam defines where the Bragg peak will occur. The materials incorporated in the phantom were chosen due to their photon equivalency and the individual stopping powers were not investigated in the original design of the phantom. For this study, the relative stopping power of each phantom material was measured to validate the overall composition of the pelvis phantom.

2.1.1 Depth Dose Scanning Procedure

A portable in-house RPC water phantom was used to take depth dose measurements at the University of Texas M.D. Anderson Cancer Center Proton Therapy Center – Houston (PTC-H). An Exradin P11 parallel plate chamber (Standard Imaging, Middleton, WI) was used as the primary scanning chamber with an Exradin A12 thimble chamber (Standard Imaging, Middleton, WI) as a reference. The gantry was set at 270° with a source-to-axis distance of 270 cm set to the inside of the window of the water phantom.

Equation 2.1 is a way to measure relative stopping powers of materials to that of water (Schaffner and Pedroni 1998). This equation was used to measure the relative stopping powers of each material used in the phantom where Δx is the shift in the percent depth dose (PDD) curve when the target material is placed in the path of the beam. The reference curve was taken with no phantom material placed in the beam path.

$$\text{Rel Stopping Power} = 1 + \frac{\Delta x}{\text{width of material}} \quad \text{Equation 2.1}$$

The sample materials were taken from the same batch used to build the pelvis phantom. This insures that the overall composition and density of the samples match the structures used to create the phantom. Each material width was measured with calipers at four separate locations. These were averaged for the width used in Equation 2.1.

The reference curve (with no phantom material in the path of the beam) was produced with a 250 MeV beam energy, range shifters for a 10 cm range and a 5 cm modulation. A phantom material was secured to the front window of the water phantom without changing any delivery conditions as seen in Figure 2.1. The same beam conditions were used to produce a modified percent depth dose curve and the phantom material was replaced. This procedure was repeated until each material had been placed in the path of the beam. A second reference curve was taken at the end of session to ensure the beam output and setup conditions had not changed during the course of measurements.

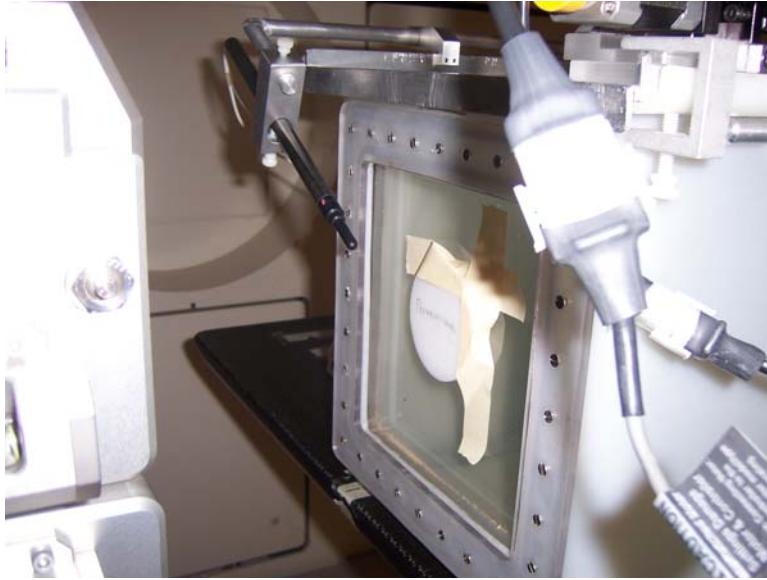


Figure 2.1: Stopping Power Measurement Setup

2.1.2 Relative Stopping Power Analysis

Each percent depth dose curve was first normalized by using the average value of 5 points centered at the nominal center of the Spread-Out Bragg Peak (SOBP) as the maximum value. Excluding the reference curve, each modified PDD curve was shifted by the width of the material placed in the path of the beam. The conditions to correctly utilize Equation 1 involved placing the materials inside the water phantom. By adding the material width to the corresponding modified PDD, the starting depth was corrected to account for placing the materials outside of the water phantom. A cubic spline interpolation was performed to estimate the value at the distal 90% for each curve. Δx was computed from the difference between the values for the material and the first reference curve. The appropriate values were then used in Equation 2.1 to calculate the relative stopping power for each material.

2.1.3 Relative Stopping Power Comparison

The PTC-H uses the Eclipse treatment planning system (TPS) (Varian Medical Systems, Palo Alto, CA) to create patient treatment plans. The TPS contains a calibration curve which converts the Hounsfield Units (HU) from the CT scanner to the relative stopping powers of human tissues. HU for each material were measured to compare with the values that are assigned by Eclipse.

A CT scan of the pelvis phantom (discussed in more detail in Section 2.2) was uploaded into Eclipse. Eight points taken across each structure and the dosimetry insert were averaged together to determine the HU for each phantom material. With the phantom material HU values, the measured relative stopping powers were plotted on the TPS calibration curve for comparison. Values taken from the literature for the phantom materials (Schneider *et al.* 1996) were also compared using the Eclipse HU values except for the PBT and High Impact Polystyrene. Literature values for these two materials were not found.

The relative stopping power comparisons were made to validate the use of the pelvis phantom in proton beams and to predict sources of discrepancies between treatment planning and treatment delivery. By comparing the measured stopping powers to the stopping powers found in the literature, it could be determined if the calculations were done correctly.

2.2 Treatment Planning

The purpose of the pelvis phantom is to evaluate the entire proton treatment process. With this in mind, all efforts were made to keep treatment planning as close to a

patient plan as possible. The phantom shell and imaging insert were both filled with room-temperature water and a special effort was made to minimize the capture of air bubbles within the phantom. The dosimetry insert was loaded with TLD and film for imaging purposes. The phantom was placed on the CT table and the laser markings were drawn on the left and right lateral surfaces as well as the anterior surface of the phantom for reference during treatment delivery setup. Small plastic BBs were placed on the laser markings to localize the phantom's position in the TPS. The pelvis phantom was scanned twice on a GE LightSpeed RT16 CT scanner at the PTC-H using the pre-set abdomen protocol. This first scan had the imaging insert loaded in the phantom and the second scan had the dosimetry insert loaded in the phantom. Once the images had been moved to the Eclipse treatment planning system the BBs were physically removed from the phantom while the laser markings were left in place. The BBs would have added material to the beam path and changed the delivered treatment from the planned treatment. Two separate treatment plans were designed from the acquired images.

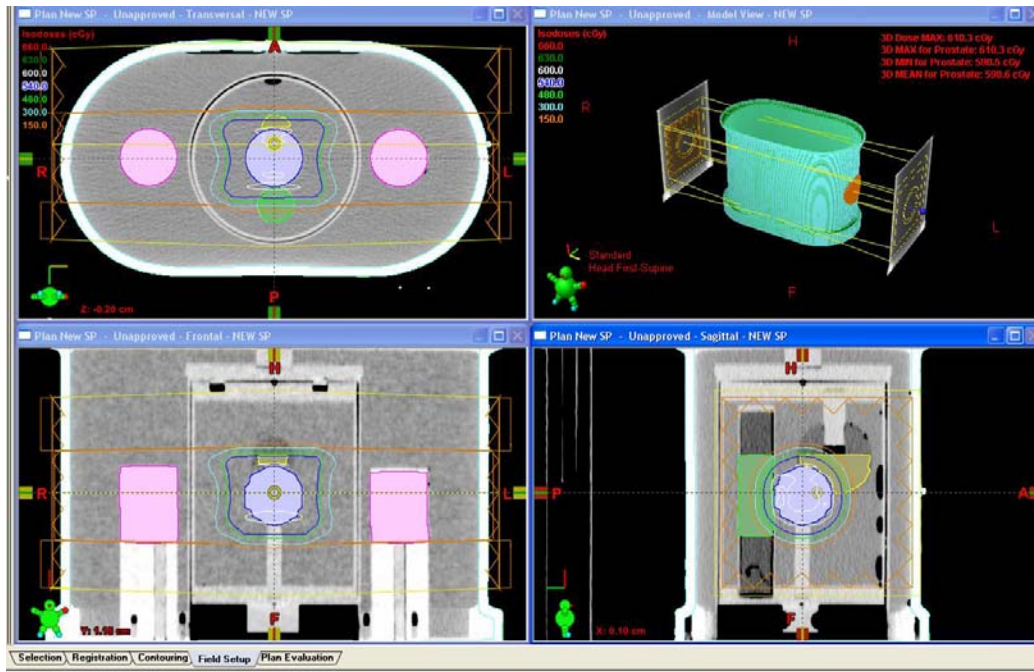


Figure 2.2: Screen capture from TPS

2.2.1 Treatment Plan 1

For the first treatment plan, the relative stopping powers assigned by Eclipse were used to calculate the dose distribution. The outer shell was contoured such that the BBs were not included in any dose calculations. The image set with the imaging insert was used for the main treatment plan as it held the necessary anatomy. The prostate, bladder, rectum and femoral heads were all contoured separately. Two lateral beams were placed so that the summed SOBPs formed a box surrounding the prostate using a preset beam template that is used for the majority of prostate treatments.

Figure 2.2 shows the pelvis phantom while being planned in Eclipse. The top left image is an axial view of the phantom with contoured structures with isodose lines surrounding the prostate. The coronal and sagittal views are on the bottom while the top right image shows the apertures on either side of the phantom.

The plan was approved for treatment by a radiation oncologist and the dose scaled

to deliver 600 cGy_{RBE} to the prostate. Points of interest were placed in the center of the target and at the location of the TLDs in each femoral head and the TPS was used to calculate the expected dose at each point of interest. The TPS was also instructed to design apertures and compensators for the two beams in Plan 1 and the information was transferred to the machine shop for construction. The beam parameters calculated by the TPS are displayed in Table 2.1

Beam Parameters - Plan 1			
Prescribed Dose - 600 cGy _{RBE}			
		Left Lateral	Right Lateral
Nominal Energy		250 MeV	250 MeV
SAD		270 cm	270 cm
Field Size		18 cm x 18 cm	18 cm x 18 cm
Gantry Angle		90°	270°
Nominal SOBP		8 cm	8 cm
Planned Distal Target Distance		24.1 cm	23.9 cm
Air Gap		10.8 cm	10.8 cm
Snout Position		30 cm	30 cm
Range Modulator		RM_27	RM_27
Isocenter Dose		299.5 cGy _{RBE}	300.8 cGy _{RBE}
Isocenter Depth		18.5 cm	18.6 cm
Isocenter Eq. Path Length		19.6 cm	19.7 cm

Table 2.1: Beam Parameters for Treatment Plan 1

The insert used to create the treatment plan and the insert used to hold the TLD and film are composed of different materials which could cause the measured dose to differ from the expected dose. To evaluate this dose difference, the CT scan of the pelvis phantom (discussed in Section 2.2) with the dosimetry insert was uploaded into Treatment Plan 1 as a “verification plan”. The proton fluence, apertures and compensators from the beams used for the original plan were copied into this verification plan and the dose from the beams incident on the dosimetry insert was calculated. The same dose points were placed on the verification plan to compare the calculated dose to the measured TLD dose.

2.2.2 Treatment Plan 2 - New SP Plan

For the second treatment plan, the measured stopping powers were substituted for the values assigned by the HU-Stopping Power calibration curve. This can be done by selecting a contoured organ and reassigning the Hounsfield Unit in Eclipse. A linear interpolation was performed to find the corresponding HU number for each measured stopping power. A new plan was created to deliver 600 cGy_{RBE} to the prostate. The same points of interest from Treatment Plan 1 were placed on Treatment Plan 2. The new aperture and compensator designs were transferred to the machine shop to be built. The same beams and points of interest were placed on the dosimetry insert to calculate the expected dose at the locations of the TLD in the same manner as with Treatment Plan 1. The beam parameters for Treatment Plan 2 are listed in Table 2.2.

Beam Parameters - Plan 2 - New SP Plan			
Prescribed Dose - 600 cGy _{RBE}			
		Left Lateral	Right Lateral
Nominal Energy		250 MeV	250 MeV
SAD		270 cm	270 cm
Field Size		18 cm x 18 cm	18 cm x 18 cm
Gantry Angle		90°	270°
Nominal SOBP		9 cm	9 cm
Planned Distal Target Distance		25.0 cm	24.8 cm
Air Gap		10.2 cm	10.3 cm
Snout Position		30 cm	30 cm
Range Modulator		RM_27	RM_27
Isocenter Dose		299.5 cGy _{RBE}	300.7 cGy _{RBE}
Isocenter Depth		18.5 cm	18.6 cm
Isocenter Eq. Path Length		20.1 cm	20.3 cm

Table 2.2: Beam Parameters for Treatment Plan 2 – New SP Plan

The effort was made to keep as many parameters between Plans 1 and 2 identical so the differences in results could be attributed to the difference in relative stopping power values used to calculate dose.

2.3 Dosimeters

The two dosimetry tools used with the phantom during irradiation are TLD capsules and Gafchromic® film. The TLD was used as an absolute dosimeter to measure point doses in specific locations. The film dose was scaled relative to the TLD dose to provide two-dimensional profiles across the sagittal and coronal planes of the phantom.

2.3.1 EBT Film

Gafchromic® EBT film was used to gather data along the coronal and sagittal

planes. Film is being a 2-D dosimeter and is able to gather spatial information as compared to TLD. The film is a light blue which darkens in the presence of radiation but is insensitive to room lighting. Figure 2.4 shows the layers used to compose the film from the white paper published for this film (ISP 2007).

Clear Polyester	97 microns
Active layer	17 microns
Surface Layer	6 microns
Active layer	17 microns
Clear Polyester	97 microns

Figure 2.3: Configuration of the Gafchromic® EBT Film

The effective atomic energy of the film is 6.98 (ISP 2007) making it close to tissue equivalent in a photon beam and an appropriate addition to the current pelvis phantom. The optical density of the exposed film is proportional to the dose to the film and it has been found that the response for Gafchromic® MD-55 film is nearly linear from 0 – 100 Gy in proton beams (Vatnitsky 1997). It is expected that the Gafchromic® EBT film has a similar response. The relative stopping power of the film was not measured in this study. The MD-55 film has also been found to be independent of energy within each batch and calibration curves created using ^{60}Co radiation, high-energy electrons and protons were observed to be near identical in this study (Vatnitsky 1997). It has also been shown that the calibration of EBT film using a 6 MV photon beam is within 2.5% of a calibration in a proton beam at 5 and 10 Gy (Nerbun 2005). Since the film is being used as a relative dosimeter, it was decided that use of the calibration curve from a photon beam was an appropriate decision.

Pieces of Gafchromic® EBT film Lot # 48022-05I (ISP Technologies, Wayne, NJ) were cut to fit in the coronal and sagittal planes of the dosimetry insert. The films were kept in black envelopes labeled by plan and trial. The films were labeled prior to irradiation for orientation purposes. The films from each trial were all cut from the same piece of film and all film irradiations were made using the same batch of film. The TLD were also from the same batch and were identified by plan, trial and location within the phantom.

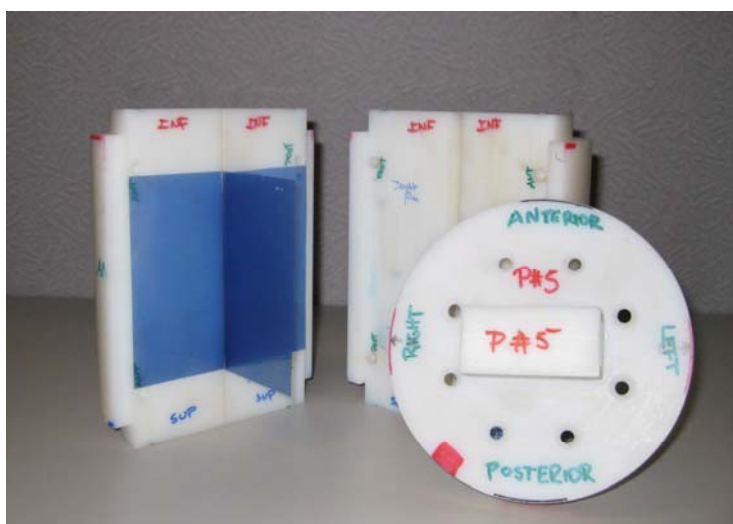


Figure 2.4: Dosimetry Insert

2.3.2 Thermoluminescent Dosimeters

For this project, capsules containing LiF TLD-100 powder were used to take absolute point measurements within the phantom. These pre-loaded capsules contain about 22 mg of powder. Double loaded capsules contain two pockets of TLD powder each with about 22 mg of powder. The double loaded capsules were used for TLD measurements.

In thermoluminescent (TL) detectors, incident radiation releases electrons from

the valence band to the conduction band and the electrons are then captured by various trapping centers (Knoll 2000). When exposed to heat, these trapped electrons are able to return to the conduction band while releasing light. A photomultiplier tube (PMT) can record the amount of light and a glow curve is produced comparing the light signal to the temperature at the time of light emission. The glow curve will have several peaks corresponding to the different trapping centers. The low temperature energy traps are not stable at room temperature and are susceptible to spontaneous recombination. The TL signal for these peaks are not reliable. By waiting to read out the TLD (usually for 10-14 days) and pre-heating the crystal, the low temperature traps are cleared leaving the stable high temperature traps which provide useful signal. The TL signal is the area under the glow curve which corresponds to the number of photons released. This signal, along with the correction factors listed in Equation 2.2 yields the dose delivered to the TLD.

$$D = T \times K_e \times K_l \times K_f \times S \quad \textbf{Equation 2.2}$$

Equation 1.4 outlines the procedure for measuring the absorbed dose, D , given to the TLD where T is the TL signal divided by the mass of the aliquot of powder, K_e is the energy correction, K_l is the linearity correction, K_f is the fading correction and S is the system sensitivity. The K factors are consistent throughout each batch of TLD and only need to be found when initially characterizing the current batch. As the RPC conducts large scale remote auditing, having the same correction factors reduces the time needed to evaluate irradiated TLD.

The energy correction factor accounts for the difference of the TLD response in energies other than the standard ^{60}Co used to commission the TLD batch. This factor is

determined by comparing the dose response of TLD in a specific beam to the response of TLD in ^{60}Co beam for the same absorbed dose (Kirby *et al.* 1992).

The linearity correction factor accounts for the supra-linearity response of the TLD batch over a range of 0-6 Gy. TLD capsules are irradiated over the designated range and a least squares fit is applied to the data set of reading versus dose. K_l is described by Equation 2.3.

$$K_l = m \times \text{raw dose} + b \quad \textbf{Equation 2.3}$$

In this equation, the raw dose is the TL reading per mg corrected for system sensitivity and fading, and both m and b are parameters which are batch specific.

The fading of the TL signal is another batch-specific quantity and is measured over time. Equation 2.4 is fitted to the measured data with the quantities a , b , c , d , and N all being batch specific parameters and X being the time in days from irradiation.

$$K_f = N / (a \times e^{-bX} + c \times e^{-dX}) \quad \textbf{Equation 2.4}$$

The TLD used in the pelvis phantom was read out at a minimum of 10 days post-irradiation to reduce the fading effect.

The system sensitivity can change for every readout session due to factors including (but not limited to) the electronics of the reader, heater characteristics and planchet reflectivity (Kirby *et al.* 1992). This factor, S , is determined by Equation 2.5 where the “prime” values are for the “standard” TLD. The standard TLD are irradiated to a known dose determined by an ionization chamber measurement.

$$S = D' / (T' \times K_{f'} \times K_{l'}) \quad \textbf{Equation 2.5}$$

The standard TLDs are read out at the beginning and end of each session so the correct S

value can be interpolated for any reading during the session and applied in Equation 2.2.

Four TLD-100 capsules (Quantaflux, LLC, Dayton Ohio) were placed within the pelvis phantom for each irradiation. Two TLD capsules were in the center of the dosimetry insert in the same location in space as the center of the prostate and one TLD capsule was placed in each femoral head in the same plane as the target TLD. The film was placed in the dosimetry insert (as seen in Figure 2.4) and was held in place by small pins. The coronal film is one solid piece while the sagittal film is cut in half to intersect at the center of the insert. The two TLD capsules fit in the center of the insert near the cross-section of the film.

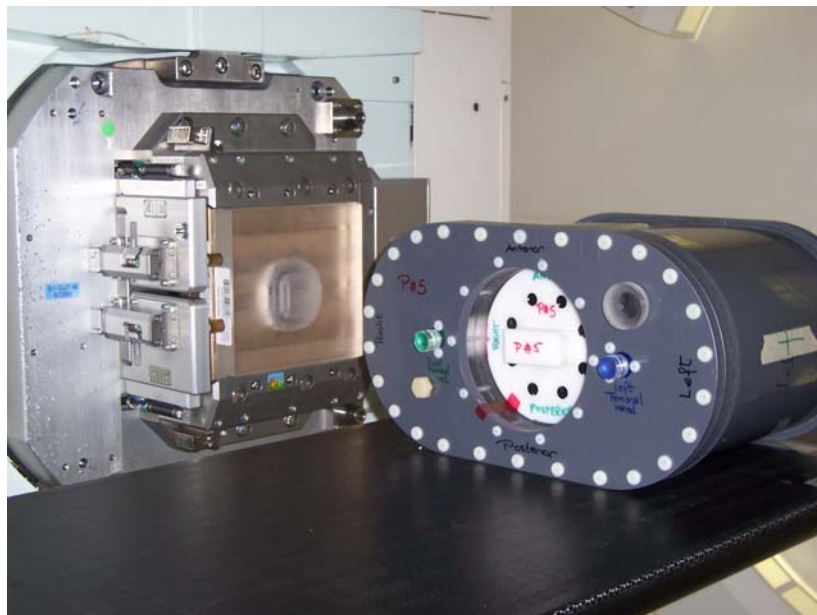


Figure 2.5: Phantom Treatment Setup

2.4 Treatment Delivery

Once the pelvis phantom was loaded with the film and TLD, the phantom was placed on the treatment table. With the gantry rotated to 270° the lasers were turned on to

set the phantom to the laser markings drawn during simulation. The lasers were used to verify the phantom's positioning between each trial to correct any movement while inserting new TLD and film. The beam parameters (listed in Tables 2.1 and 2.2) and the monitor units were entered into the computer console for beam delivery. Each treatment was performed with two fields in one fraction. For each treatment plan, 3 irradiations were made using the pelvis phantom.

2.4.1 Monitor Unit Calculation

The monitor units (MU) for each beam were entered into the console for the simplest delivery of the two treatment plans. The record and verify system was not used to expedite treatment delivery. The plan was prescribed to deliver 600 cGy_{RBE} but the goal was to deliver a dose of 600 cGy to the TLD at the target. For 600 cGy to be delivered to the TLD at the target, the monitor units were calculated to deliver 660 cGy_{RBE} to account for the clinical relative biological effectiveness value of 1.1 for proton therapy.

The monitor unit calculation at the PTC-H utilizes several factors including a relative output factor, range shifter factor, spread out Bragg peak factor, and an inverse square factor (Sahoo *et al.* 2008). Any change from the reference conditions listed in Table 2.3, produces a change in the respective output factor. The machine is calibrated using the IAEA TRS 398 protocol (Andreo *et al.* 2000). These factors can be found in reference tables created from data taken during commissioning.

Energy	250 MeV
Range	28.5 cm
SOBP	10 cm
Range Shifter	none
SDD	270 cm

Table 2.3: Dosimetry Reference Conditions

Equation 2.6 was used to calculate the monitor units for treatment

$$MU = \frac{\text{PointDose(cGy)}}{\text{Rel. OF} \times \text{Range Shifter Factor} \times \text{SOBP Factor} \times \text{ISQ} \times \text{Comp. Factor} \times \text{SOBP OCF}}$$

Equation 2.6

where Rel. OF refers to the relative output factor, ISQ refers to the inverse square factor, Comp. Factor refers to the compensator factor and SOBP OFC refers to the SOBP off-center factor. The aperture factor was not considered in the calculated MU; however, the dependence of output on aperture size is known to be very small and this omission was shown to contribute less than a 1% error to the total calculation.

2.5 Dosimetry Data Analysis

The two dosimetry tools with the phantom during irradiation are TLD capsules and Gafchromic® film as mentioned in Section 2.3. The TLD was used as described in Chapter 1 to determine point doses in specific locations. The film dose was scaled relative to the TLD dose to provide two dimensional profiles across the sagittal and coronal planes of the phantom.

2.5.1 TLD Registration

The dimensions of phantom insert were measured from the CT scan of the phantom. Five points on the imaging insert were chosen: the superior edge of the target, the posterior edge of the rectum, the center of the target, the right edge of the target and the inferior edge of the target. The center coordinates were designated as (0,0,0). From the center of the physical insert, the coordinates of the TLD were measured. All of the coordinates were recorded in a spreadsheet which is uploaded into CERR (Deasy *et al.* 2003). Once the treatment plan is uploaded to CERR, the registration can be performed using the 5 points described above. Once registered, the position of the measured dose from the TLD can be correlated with the dose profiles from the TPS.

2.5.2 Film Dosimetry

The EBT film was cut to fit in the phantom with one piece of film through the coronal plane and two smaller pieces through the sagittal plane. The CT scan of the phantom with the film-loaded dosimetry insert in place was used to check for any air gaps along the planes of the film. Extra pieces of film were fitted in the dosimetry insert to try and eliminate these air gaps.

The film was calibrated with a Varian 2100 linear accelerator (Varian Medical Systems, Palo Alto, CA). One piece of film was cut into 9 smaller square pieces of film and irradiated at 9 levels ranging from 50-1350 MU. This was done using 6 MV photons, a 35 cm x 35 cm field size and an output factor of 1.075 giving doses which ranged from 53.75 cGy to 1451.25 cGy. Each piece of film was pre-labeled to preserve orientation and to later identify the dose given to each individual cutout. The film was scanned with a CCD Microdensitometer for Radiochromic Film Model CCD100 (Photoelectron Corporation, Lexington, MA). A background film from this batch of film was used to

acquire a flat field image and a grid with 1 cm blocks was used for spatial calibration of the system. Using these two corrections, the film was placed in the densitometer and the images were saved as FIT files for later evaluation.

The average optical density of each piece of the calibration film was measured with ImageJ software (Rasband 1997-2009). A calibration curve to convert optical density into dose was created for each of the 3 trials and a cubic polynomial fit was applied. This fit was used to convert the films from the pelvis phantom into dose measurements. Error bars reflecting the standard deviations of the dose values were placed on the calibration curves for comparison between the trials. Any points outside of the corresponding error bars from the other two calibration curves would raise a concern about the film's irradiation and subsequent analysis.

2.5.3 Film Registration

To register the position of the film to the TPS, four pin pricks were placed on each film. These pins were inset in the dosimetry insert and were also used to hold the film in place. A template was created for the pin pricks for each plane of the film and the coordinates of each pin were recorded in a table. These data were stored in a spreadsheet that was recalled when registering the film in an in-house program which supplements CERR. This software also included a section to place the TLD measurements and would automatically scale the film dose to these points. The pin holes in the scanned film were carefully selected and then uploaded into CERR for registration with the TPS. The dose profiles from film were compared to the treatment plan to check for agreement in the dose surrounding the prostate. The profiles were taken through the center of the coronal plan from left to right and from superior to inferior. The sagittal profiles went through the

center of the film in the AP PA direction and were off-center 2 mm from superior to inferior. This was due to the sagittal film being cut in the center to intersect with the coronal film. These selected dose profiles through the film and TPS are exported for further analysis as discussed in Section 2.6.2.

2.6 Treatment Procedure Evaluation

2.6.1 TLD Comparison

The TLD for the phantom measurements were read out 14 days post irradiation for Plan 1 and 10 days post irradiation for Plan 2. The readings were inserted in an Excel worksheet which accounts for all of the correction factors listed in Equation 2. The measured value was directly compared to the expected dose at the corresponding point from the TPS for a ratio. For Plan 1, this was done for the main plan on the imaging insert and the verification plan for the dosimetry insert so the two inserts could be compared. A ratio value from 0.95 – 1.05 was considered a passing value. The TLD for each plan were also evaluated for reproducibility using the coefficient of variation (COV) and a value no greater than 3% was considered a passing value.

A one-sample t-test was also performed on the TLD data to check for statistical significance with $\alpha = 0.05$ as the significance level. The null hypothesis, μ_0 , was defined to be equal to 0.949 and corresponds to the null hypothesis in Equation 2.7. The hypothesis proposed earlier required $\mu > 0.949$. The standard deviation, s , the total number of values, n , and the mean for the three trials, \bar{x} , were also used to calculate the t-test (Rosner 2006).

$$t = \frac{\bar{x} - \mu_0}{s/\sqrt{n}} \quad \text{Equation 2.7}$$

The Excel function TDIST was utilized to calculate the corresponding p -value.

The p -value needed to be less than 0.05 for statistical significance. If the p -value was greater than 0.05, then the results would not be considered statistically significant and the null hypothesis would be accepted (Rosner 2006).

2.6.2 *Beam Profiles Comparison*

To evaluate the accuracy of the treatment delivery, the beam profiles from the film were compared to the corresponding beam profiles from the TPS. These profiles were exported into an Excel spread sheet and plotted for visual inspection. The maximum and minimum dose values along the dose gradients of the film profile were used to determine three locations along each profile: the 75%, 50% and 25% dose points. A linear regression was taken over the portion defined by 80% and 20% of the profile edge so a formula could be derived for both the film and TPS dose profiles. The doses at the three previously designated points were calculated for each profile and the displacement between each set of doses was calculated. The average displacement for these three points defined the displacement between the two profiles. A displacement no greater than 3 mm was considered as having passed.

2.6.3 *Treatment Plan 2 Quality Assurance*

The treatment plan for the new stopping powers was also checked using the patient QA for normal clinical treatments. The beams from the treatment plan were placed in a verification plan with a water phantom in place of the pelvis phantom in the same manner described in Section 2.2.1. The dose profiles were calculated and a profile through the center of the field along the coronal plane was exported.

Much like the process for measuring relative stopping powers described in Section 2.1.1, the water phantom was set to scan along the beam. Instead of an open field,

the apertures created for the plan were in place. The beam parameters listed in Table 2.2 were set and the beam was turned on for the duration of the scan. This was done for both fields, right and left lateral, with the gantry in the corresponding position. The water phantom was set to have the window facing the snout of the machine.

The data from the scans were compared to the data from the TPS by finding the center of the SOBP for both scans. The scans were then compared relative to their respective center points and the shift of the distal 90% depth dose point was measured using a cubic spline interpolation in the same manner as in Section 2.1.2. Any significant shift between distal 90% points of the depth dose curve would indicate a difference from the plan to treatment.

Chapter 3

Results and Discussion

3.1 Phantom Material Stopping Powers

3.1.1 Relative Stopping Power Analysis

The depth dose scan obtained with each of the materials tested attached to the front of the water phantom was compared with the depth dose scan obtained with the material removed. Figure 3.1 shows the percent depth dose curve with nylon in the beam (shown in blue) and the curve obtained in water (shown in pink). Nylon was the material used to represent the prostate.

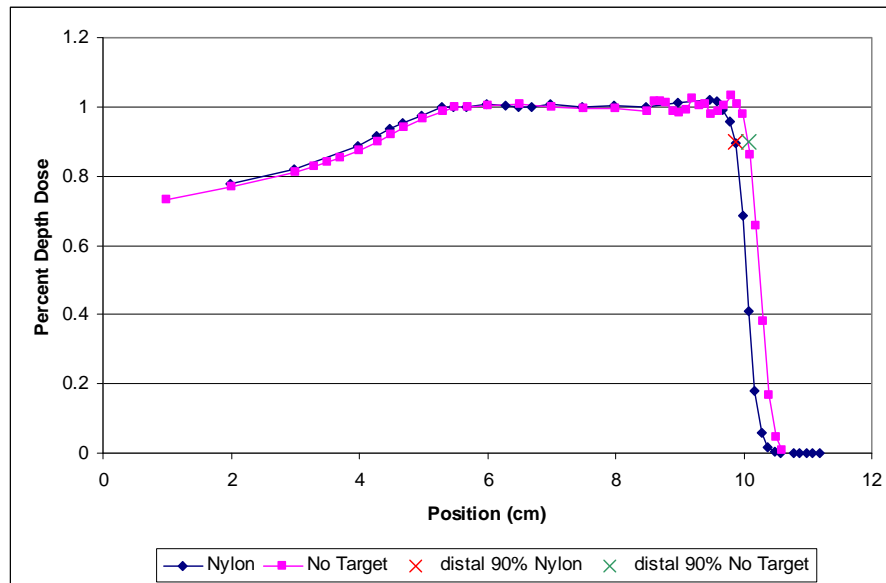


Figure 3.1: Depth Dose Curve with and without Nylon

The difference in the distal ends of the SOBP shows the difference in the penetration of the beam due to the difference in the stopping power of the materials in the beam path. The “x” placed on the distal end of the peak marks the 90% depth dose point as calculated from the cubic spline interpolation. Since the distal 90% of the beam is used

to define the end of the range for a SOBP, it was chosen as a consistent point to measure. The values for Equation 2.1 are listed in Table 3.1 for all of the phantom materials to calculate the measured relative stopping powers.

Material	Width (cm)	Shift (cm)	Rel. SP
Nylon - Prostate	0.979	0.198	1.20
PVC - Shell	0.549	0.125	1.23
PBT - Bone	0.693	0.142	1.21
HI Polystyrene - Dosimetry Insert	1.46	0.096	1.07
Polyethylene - Bladder	1.05	-0.003	0.997
Acrylic - Bone Marrow	1.67	0.353	1.21
Wax - Rectum	2.42	0.029	1.01

Table 3.1: Relative Stopping Powers

The measurements of the thickness of each material had an absolute error of 0.005 mm for each side of the materials and a total error of 0.01 mm or 0.001 cm. The material samples were not of uniform thickness so the uncertainties of thickness for each side were added together for the total error. The scanning system is believed to be accurate within 0.1 mm giving an uncertainty for the relative SP on the order of 0.01.

3.1.2 Stopping Power Comparison

The stopping powers were compared to the literature values described in Schneider *et. al.* and were plotted in Figure 3.2 along with the HU calibration curve for the Eclipse TPS and the measured values from Table 3.1. The HU were decided using the procedure outlined in Section 2.1.3.

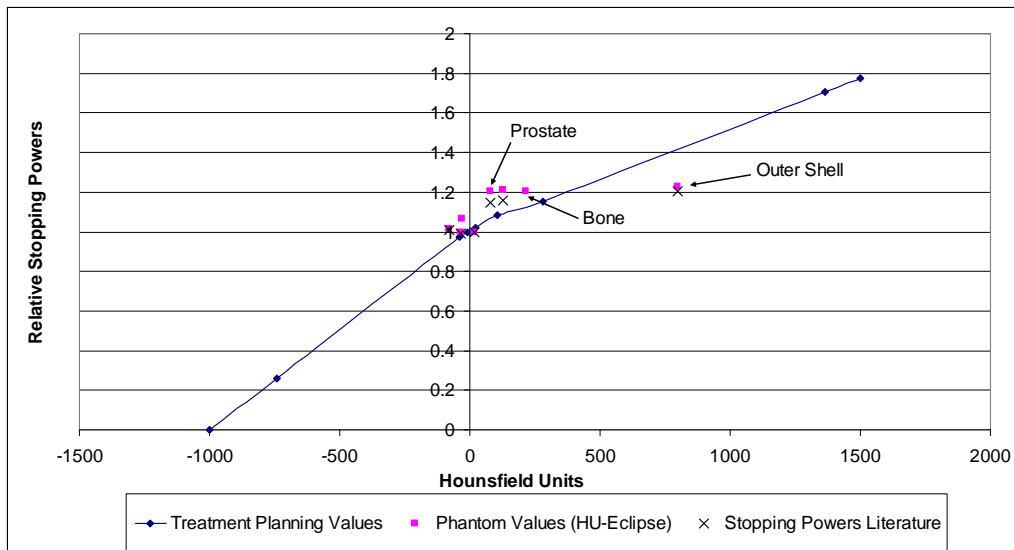


Figure 3.2: Comparison of Relative Stopping Powers

The measured stopping powers were all less than 5% different than the corresponding literature values. For this reason, the measured stopping powers were considered valid as differences in material composition and density could account for the differences in the stopping powers. The measured stopping powers for several of the materials, including the target material, were nearly 10% different from the stopping power values used in the TPS. For this reason, two plans were created to quantify the differences this caused in phantom irradiation.

The difference in the stopping powers values for the phantom materials from the TPS could impact the comparisons of the calculated and measured dose by greatly affecting the measured dose. If the two treatment plans deliver significantly different results, it would be necessary for institutions to correct the TPS for the actual stopping powers of the materials. Otherwise, any failure to meet the specified requirements to pass the phantom evaluation could be attributed to the material stopping powers and not the institution's treatment procedures.

3.2 Treatment Planning

3.2.1 Treatment Plan 1

The TPS was used to generate a plan using the parameters that were listed in Table 2.1. The dose was calculated with the beams placed on both the imaging insert and again with the beams placed on the dosimetry insert. The results are shown in Table 3.2.

Dose Points	Calc. Dose (cGy _{RBE}) Imaging Insert	Calc. Dose (cGy _{RBE}) Dosimetry Insert
PTV Right	600.2	596.0
PTV Left	600.2	596.0
Right Femoral Head	247.3	249.6
Left Femoral Head	243.8	245.2

Table 3.2: Calculated Dose Points Plan 1

The TPS automatically planned using the clinical RBE value of 1.1. To have the physical dose to the target be 6 Gy, the biological dose to the phantom was equal to 6.6 cGy_{RBE}. It is convention to irradiate the phantom TLD and film to a target dose of 6 Gy. Dose delivery needs to be carefully documented to correctly estimate the dose delivered to the TLD.

3.2.2 Treatment Plan 2 – New SP Plan

The measured stopping powers used to create the second treatment plan are shown in Table 3.3 and are graphically represented in Figure 3.3.

Material	CT Values Corrected	CT Values Original
Nylon - Prostate	376 HU	77 HU
PVC - Shell	427 HU	800 HU
PBT - Bone	384 HU	215 HU
Polyethylene - Bladder	-10 HU	-34 HU
Wax - Rectum	18 HU	-80 HU

Table 3.3: Plan 2 CT Values

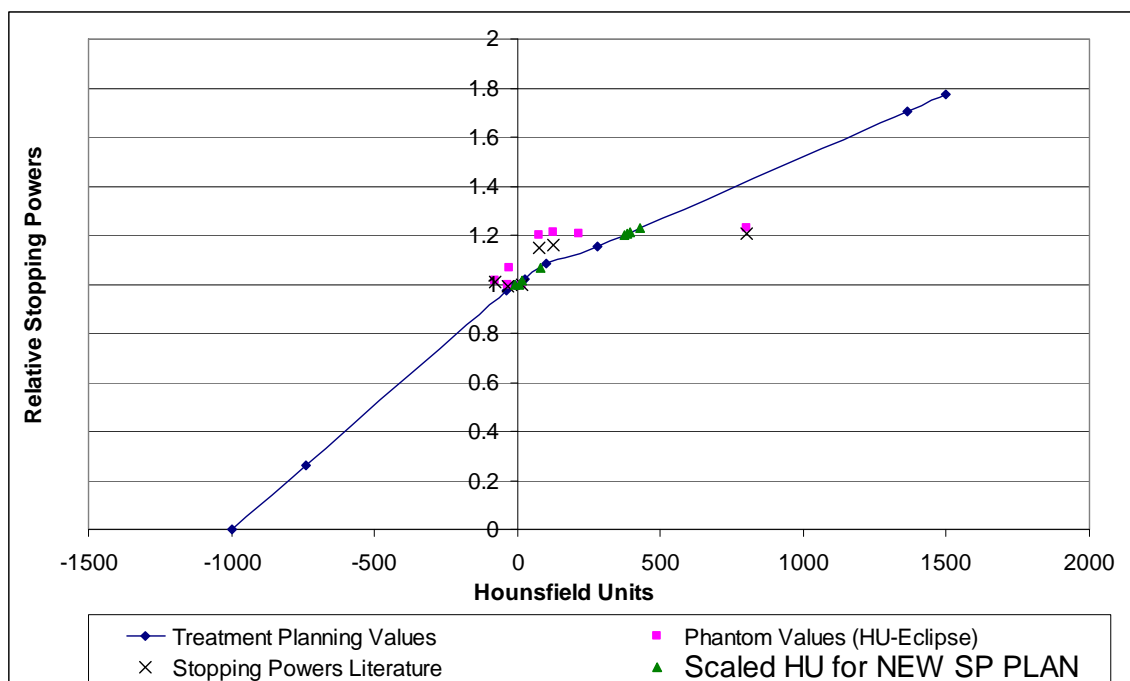


Figure 3.3: Revised SP Calibration Curve

Figure 3.3 shows how the measured stopping power values in pink are shifted laterally onto the Eclipse system's curve depicted by the green triangles. By overriding the HU in the TPS, the measured SP values were instead being used to plan the treatment and to calculate the dose distribution. The calculated doses for the new stopping powers are shown below in Table 3.4.

Dose Points	Calc. Dose (cGy_{RBE}) Imaging Insert	Calc. Dose (cGy_{RBE}) Dosimetry Insert
PTV Right	600.2	594.9
PTV Left	600.2	594.9
Femur Right	252.2	250.4
Femur Left	248.1	247.8

Table 3.4: Calculated Dose Points Plan 2

When the dose distribution was calculated on the dosimetry insert, the dose to the PTV was reduced by about 1% for both plans. As the dosimetry insert is slightly denser than water with a larger stopping power (refer to Table 1.1 and Table 3.1), a small decrease in dose was expected. The change in the femoral heads was not expected since the femoral heads are fixed in the phantom shell and do not change with different inserts. The difference in the calculated doses to the femoral heads between the two inserts was again within 1%. This difference could be simply from a re-calculation in general (assuming the calculation algorithm changes minutely with every calculation) or could be caused by the change in the interface at the insert.

3.3 Treatment Delivery

The monitor units (MU) were calculated to deliver the treatment to the pelvis phantom using Equation 2.2. The exact factors and final number of MU for both plans are listed in Table 3.5. These factors correct for the differences between the reference conditions (Table 2.3) and the beam parameters for treatment (Table 2.1 and Table 2.2).

	Plan 1			Plan 2 - New SP Plan	
Beam	Left Lateral	Right Lateral		Left Lateral	Right Lateral
Relative OF	1.000	1.000		1.000	1.000
Range Shifter Factor	0.967	0.968		0.972	0.973
SOBP Factor	1.057	1.057		1.028	1.028
ISQ Factor	1.000	1.000		1.001	1.000
Compensator Factor	1.000	1.000		1.000	1.000
SOBP OCF	1.000	0.997		1.001	0.999
MU Required	294.3	293.6		300.3	299.7

Table 3.5: Monitor Unit Calculation

The MU increased from Plan 1 to Plan 2 which suggests the materials in the phantom have higher stopping powers than the TPS calibration curve would assign. A difference was expected as the TPS uses a calibration curve designed for human tissue and not plastic material. Figure 3.3 shows the difference between the stopping powers used to calculate the two plans. The pink squares represent the stopping powers of the phantom materials at the HU assigned by the TPS. As previously mentioned in Section 3.1.2, five of the materials have noticeably larger stopping powers than the assigned value (as seen by the blue line representing the TPS calibration curve).

3.4 Dosimetry Data Analysis

The dosimetry tools for the phantom were evaluated as a system to verify the treatment planning, setup and delivery to the pelvis phantom. The TLD irradiations were used as the absolute dosimeter and the film dose was scaled to these dose points for a relative measurement.

3.4.1 Thermoluminescent Dosimeters

The TLD batch used in the pelvis phantom was named B07 and had been commissioned prior to the start of this project. Equation 2.2 listed the correction factors

used for the final dose calculation with Equations 2.3-2.5 detailing the quantities which go into these correction factors.

The linearity correction factor (Equation 2.3) is derived from the least-squares fit described in Section 2.3.2. The slope (m) for B07 was -0.00027842 and the y-intercept (b) was 1.08353. The fading correction factor (Equation 2.4) was a more complicated fit and the batch-specific values are listed in Table 3.6.

N	1.3493
a	1.2815
b	0.00010885
c	0.06781
d	0.071908
X	Days From Irradiation

Table 3.6: Fading Correction Constants

3.4.2 TLD Registration

The TLD was registered to the phantom plan through designated points that were measured on the CT scan set to 2 mm slice widths. The five landmarks were chosen since they are easily visible on the scan and are not in the same plane. Three of the points shown (posterior edge of the rectum, the center of the prostate and the right edge of the prostate) were in the same center plane while the other two points moved superior and posterior in the phantom. Table 3.7 lists the coordinates set from the initial CT scan during commissioning in millimeters while Figure 3.4 is a snapshot of the plan registration showing points contained in the same plane of the treatment plan. Once the plan was registered, the two TLD locations within the dosimetry insert were known as being 4 mm right posterior and 4 mm left anterior from the designated center of the

phantom.

3D coordinates on Imaging Insert					
	edge target superior	edge rectum posterior	center	edge target right	edge target inferior
x	0	0	0	25	0
y	0	-56.1	0	0	0
z	25	0	0	0	-25

Table 3.7: 3D Coordinate Registration

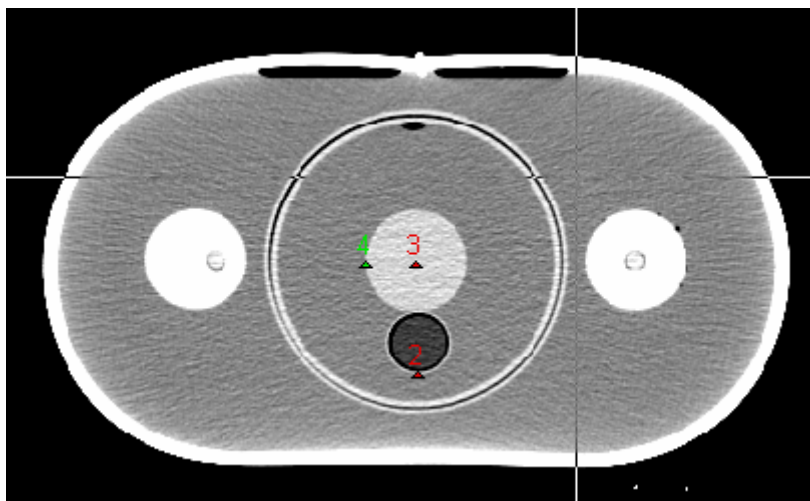


Figure 3.4: Treatment Plan Registration

The registrations were evaluated by the root mean square (RMS) value of the differences between the known location of a point and its coordinates on the CT. For Plan 1 the RMS was 0.87 mm and for Plan 2 – New SP the RMS was 0.9 mm. A RMS value less than 1 mm was deemed an acceptable registration. With this registration in place, the coordinate locations of the film pin holes were also set in the plan. When the film is registered, the two sets of pin holes (the set selected on the film and the set known from the plan registration) were fused so the measured radiation and the planned radiation were connected.

3.4.3 *Film Dosimetry*

The Gafchromic® EBT film is the preferred type of film to use for phantom irradiations since it reliably gathers a large amount of information and does not need wet processing. As this type of film is not sensitive to room light, it can be cut into smaller pieces that are shaped to fit the phantom.

There have been studies to address the suitability of radiochromic film as a dosimeter in protons (Vatnitsky 1997; Nerbun 2005). Radiochromic film typically under-responds at the distal end of the SOBP which is problematic for range measurements. The relative stopping power of the film has not been measured so it is not known whether having the film in the beam path would quantifiably change the range of the protons along the plane of the film. More studies would have to be made in the future to assure that film is an acceptable medium for this phantom in proton therapy.

The film calibration curves are shown in Figure 3.5. Trial 3 (shown in blue) was used for the calibration of the irradiated film. The standard deviation of each measurement was no more than 0.006 and the COV for the calibration curve used in the study centered around 0.8%. The polynomial fit shown in Equation 3.1 was applied to the data with dose as a function of optical density.

$$y = 2861.6x^3 - 1455x^2 + 586.26x \quad \textbf{Equation 3.1}$$

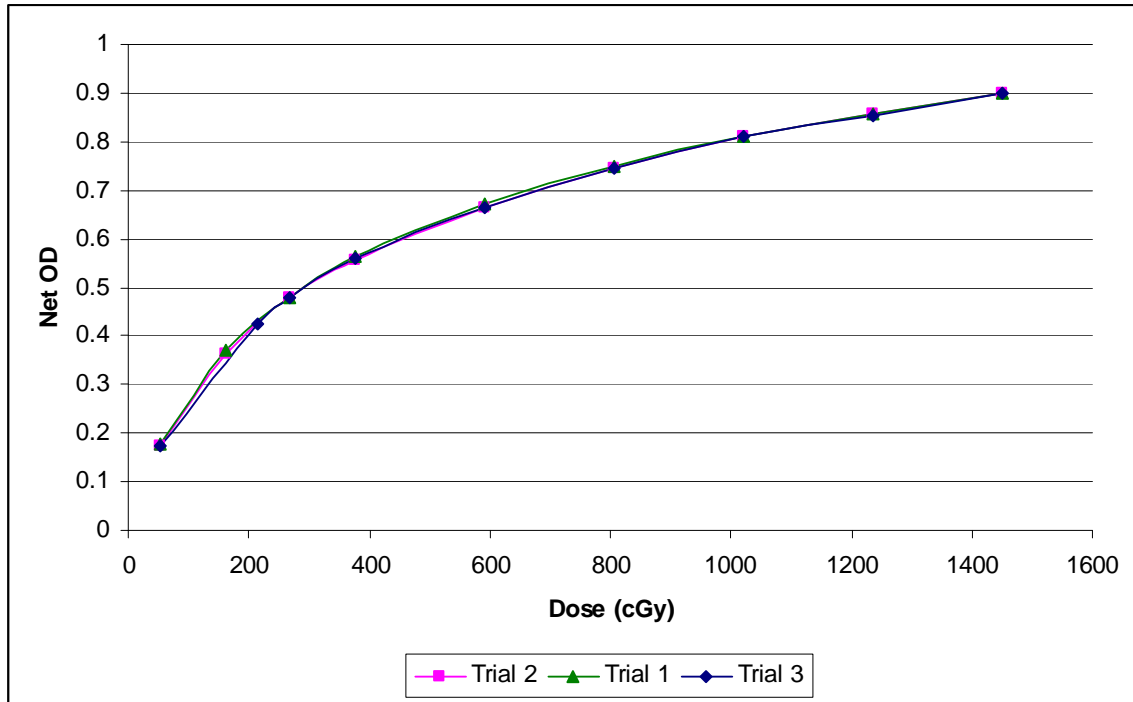


Figure 3.5: Film Calibration Curve

In the RPC system, the TLD are used for dose point measurements and the film dose is scaled to these points. The 3% change seen in calibration curves for the proton beams and the photon beams (as stated in Section 0) would have been a greater concern had the film been used to directly measure the dose profiles. The low energy dependence of the film within batches provided confidence that the calibration using a 6 MV photon beam would not significantly affect the data. One concern was the under representation of dose seen at the distal end of the range by 5-10 % (Vatnitsky 1997). With the shifts between the planned and measured profiles being taken from the 75% - 25% region, this under-response of the film should not affect our measured displacements between the measured and calculated profiles.

3.4.4 Film Registration

The film was registered to the treatment plan by four pin pricks created by the dosimetry insert which can be seen in Figure 3.6. The coordinates of the pin pricks on the film were recorded and are shown in Table 3.8. Any setup error made with the phantom would appear once a comparison of the measured profiles to the calculated profiles was performed since the physical coordinates of the film would not match the expected coordinates in reference to the designated center of the phantom. Care was taken when loading and unloading the film from the dosimetry insert to keep from “doubly-pricking” the film. This can cause a mis-registration that can result in false range data from the measured profiles.

Film coordinates sagittal					TLD coordinates sagittal	
	superior posterior	superior anterior	inferior posterior	inferior anterior	right posterior	left anterior
x	0	0	0	0	0	0
y	-47.8	54	-56.9	48.5	-4	4
z	55.1	55.1	-48.5	-51.9	0	0
Film coordinates coronal					TLD coordinates coronal	
	superior left	superior right	inferior left	inferior right	right posterior	left anterior
x	-42	52	-53.6	47	4	-4
y	0	0	0	0	0	0
z	55.4	46	-48.1	-50	0	0

Table 3.8: 2D Film Registration

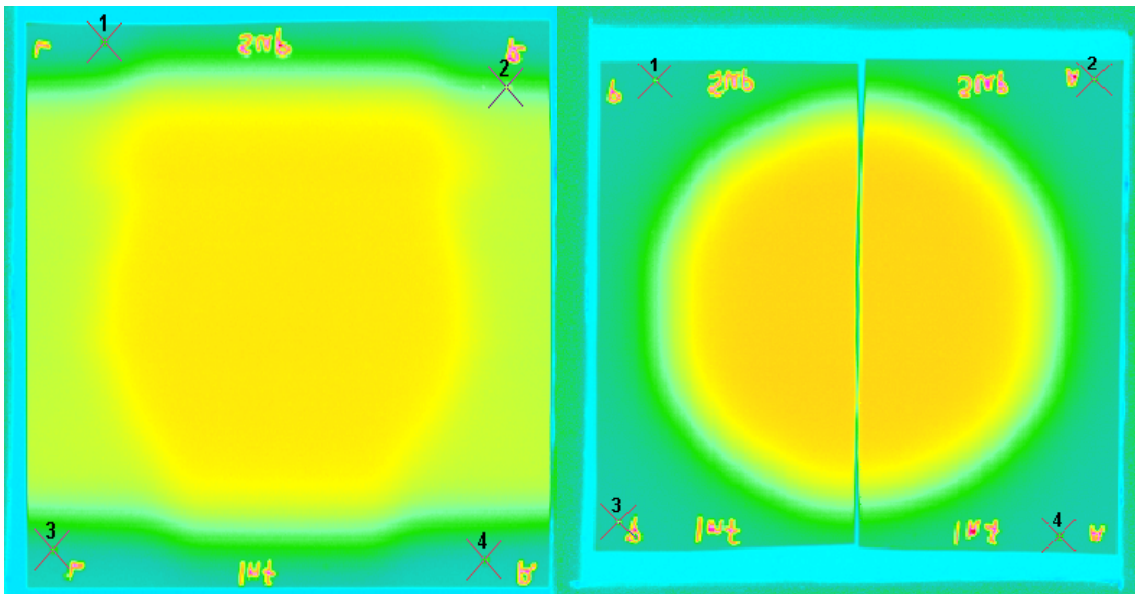


Figure 3.6: Film Registration Points

Each film was uploaded into our in-house software for registration. The phantom name was selected along with the plane of the film. For example, Figure 3.6 was uploaded as a pelvis phantom with the coronal film on the left and the sagittal films on the right. The two sagittal film pieces were scanned and registered together. The “X” marks on the film were placed on the pin pricks using a magnified view of the film. These marks should align with the coordinates listed in Table 3.8. At this point, the film is registered to the phantom, converted to dose and scaled relative to the TLD point measurements. The phantom was registered to the treatment plan and to the film measurements. Dose profiles from the measured data and that calculated data can now be taken through the same planes.

3.5 Treatment Procedure Evaluation

3.5.1 TLD Comparison

The TLDs were read out 10 and 14 days post irradiation to lessen the effects of fading on the dose calculations. Each TLD capsule contained 2 aliquots of TLD. The 2

readings were averaged together to calculate the dose to the point of measurement. The measured TLD were compared to measured beam data from the use of both inserts. The CT scan of the phantom holding the imaging insert was used to create the treatment plan and these beams and dose points were placed on the image set from the dosimetry insert.

Table 3.9 shows the TLD results from the 3 irradiations of Plan 1, the calculated dose from both inserts and the dose ratios.

	Dose Points	Meas. Dose (cGy) TLD	Calc. Dose (cGy) Imaging Insert	Calc. Dose (cGy) Dosimetry Insert	Meas./Calc. Dose Imaging Insert	Meas./Calc. Dose Dosimetry Insert
Trial 1	PTV Right	589.8	600.2	596.0	0.983	0.990
	PTV Left	595.1	600.2	596.0	0.992	0.999
	Femur Right	242.1	247.3	249.6	0.979	0.970
	Femur Left	240.4	243.8	245.2	0.986	0.980
Trial 2	PTV Right	591.8	600.2	596.0	0.986	0.993
	PTV Left	592.8	600.2	596.0	0.988	0.995
	Femur Right	241.3	247.3	249.6	0.978	0.967
	Femur Left	240.3	243.8	245.2	0.986	0.980
Trial 3	PTV Right	589.6	600.2	596.0	0.982	0.989
	PTV Left	590.6	600.2	596.0	0.984	0.991
	Femur Right	244.2	247.3	249.6	0.988	0.978
	Femur Left	238.2	243.8	245.2	0.977	0.972

Table 3.9: TLD Data from Treatment Plan 1

The column specifying the Measured/Calculated dose for the imaging insert is the ratio used to designate a passing dose comparison. The imaging insert was used for the CT simulation of the pelvis phantom and is the ideal candidate to use for the calculated dose

values. All of the measured planned target volume (PTV) values were well within 5% of the calculated dose from the TPS.

The pelvis phantom is intended for use by institutions to evaluate the treatment process for proton therapy. The phantom will be mailed pre-loaded with the dosimeters and is intended for one dose fraction before it is returned to the RPC. The phantom will need a CT simulation with the imaging insert for planning but it is not necessary to do a second scan for the dosimetry insert. Placing the beams on the dosimetry insert to calculate the expected dose does marginally improve (0.7%) the dose ratio. This is expected since the actual treatment is delivered to the dosimetry insert and not to the imaging insert. One option for compensating for the differences in calculated dose is to modify the pass criteria by 1% as 0.99 ratio is expected to be the best match between the measured and calculated dose.

It was expected that changing the calibration curve of the TPS to account for the actual stopping powers of the materials comprising the pelvis phantom would improve the dose comparison as it would provide a more accurate calculation by the TPS. The TLD results from Plan 2 are shown in Table 3.10.

	Dose Points	Meas. Dose (cGy) - TLD	Calc. Dose (cGy) - Imaging Insert	Calc. Dose (cGy) - Dosimetry Insert	Meas./Calc. Dose - Imaging Insert	Meas./Calc. Dose - Dosimetry Insert
Trial 1	PTV Right	575.9	600.2	594.9	0.960	0.968
	PTV Left	567.6	600.2	594.9	0.946	0.954
	Femur Right	241.4	252.2	250.4	0.957	0.964
	Femur Left	239.6	248.1	247.8	0.966	0.967
Trial 2	PTV Right	572.1	600.2	594.9	0.953	0.962
	PTV Left	565.6	600.2	594.9	0.942	0.951
	Femur Right	241.2	252.2	250.4	0.956	0.963
	Femur Left	241.2	248.1	247.8	0.972	0.973
Trial 3	PTV Right	578.9	600.2	594.9	0.965	0.973
	PTV Left	573.4	600.2	594.9	0.955	0.964
	Femur Right	241.1	252.2	250.4	0.956	0.963
	Femur Left	240.9	248.1	247.8	0.971	0.972

Table 3.10: TLD Data from Treatment Plan 2

The measured dose from Plan 2 was on average 3% lower than its counterparts in Plan 1. Two of the TLD measurements (PTV Left in trials 1 and 2) differed more than 5% from the calculated measurements. These did not pass the set criteria of 5%/3mm. By placing the beams to the dosimetry insert, all of the measured dose points come within the 5% range of the calculated dose. Looking at the film data brings more information to determine what changes the new stopping power values have created in the treatment plan and delivery.

The lower TLD values were not expected from this plan. With the custom stopping power measurements in the calculation, the calculated and measured doses were expected to be nearly the same value. The dose difference actually increased when

compared to the first plan which did not account for the materials not being proton equivalent. It is not known if the TLD dose is a result of incorrect stopping power measurements or if the TLD do not respond as expected in a phantom of this size for protons. TLD irradiated in this phantom in other studies have been consistently 3 – 5% lower than the expected value.

The TLD measured dose from each of the 3 trials for each plan were averaged together to measure the COV between the trials.

	Plan 1				Plan 2			
	PTV Right	PTV Left	Femur Right	Femur Left	PTV Right	PTV Left	Femur Right	Femur Left
Predicted Dose (cGy)	600.2	600.2	247.3	243.8	600.2	600.2	252.2	248.1
Meas. Dose Average (cGy)	590.4	592.8	242.5	239.6	575.6	568.9	241.2	240.6
COV	0.21%	0.38%	0.62%	0.52%	0.59%	0.71%	0.06%	0.35%
Measured/Calculated Dose	0.984	0.988	0.981	0.983	0.959	0.948	0.957	0.970

Table 3.11: Average Dose Across 3 Trials

The COVs for the PTV dose measurements were both less than 0.4% while the COVs for the femoral head dose measurements were less than 0.7% (as seen in Table 3.11). Plan 2 also had a COV under 0.8% for the PTV and 0.4% for the femoral heads. The small variations between the trials show the phantom is able to reproduce TLD point measurements for a single plan. The reproducibility of the phantom measurements needs to be less than 3% to be able to securely use the phantom as an auditing tool.

A one-sample t-test was applied across the TLD data to check for statistical

significance. This was done for each TLD value across the 3 trials. Other than PTV left for Plan 2 (which was also the only dose measurement to be greater than 5% for two out of three trials) all of the TLD measurements had a p -value < 0.05 and were deemed statistically significant.

3.5.2 Dose Profile Comparison

The dose profiles from the film were plotted along with the profiles taken from the TPS to compare dose profiles delivered during treatment. The fall-off regions along the edge of the dose profiles were characterized by a linear regression from the 80% to 20% dose levels.

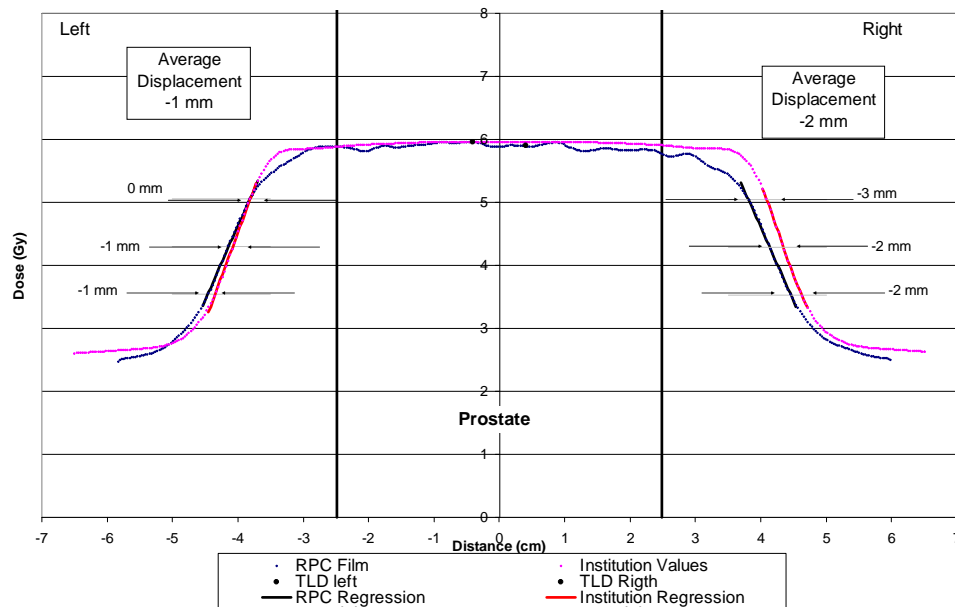


Figure 3.7: Plan 1 Trial 1 Right-Left Profile – Coronal Plane

Figure 3.7 shows the dose profiles along the beam path on the coronal plane. The displacement between the measured and calculated profile is shown at the 75%, 50% and 25% levels. The average of these displacements was taken as the total displacement

between the profiles. For Plan 1, the right-left profile for all of the trials showed a displacement that was less than 3 mm. This direction is important as it is in the direction of the beam. The edges of the dose profiles correspond with the distal end of the range of the proton beam in this view. The plots from Trial 2 and Trial 3 can be viewed in the Appendix.

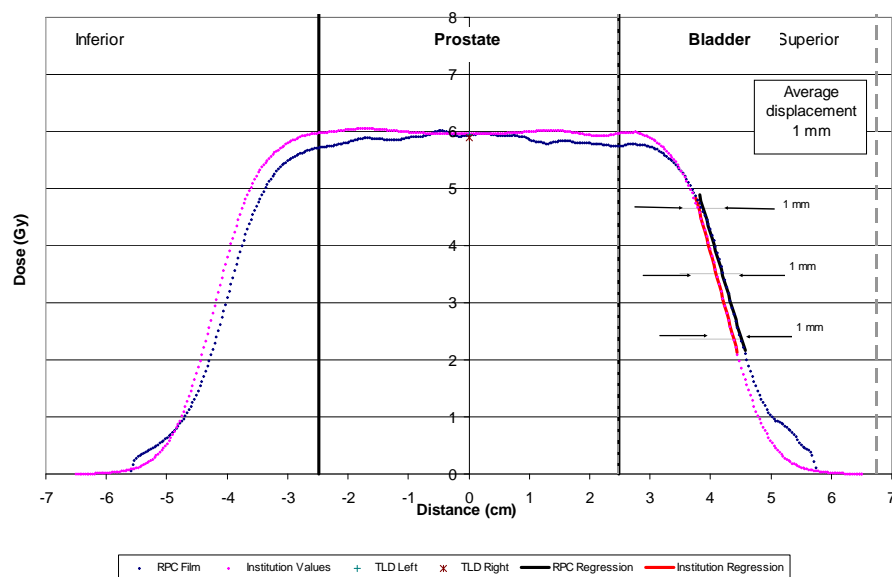


Figure 3.8: Plan 1 Trial 1 Superior-Inferior Profile – Coronal Plane

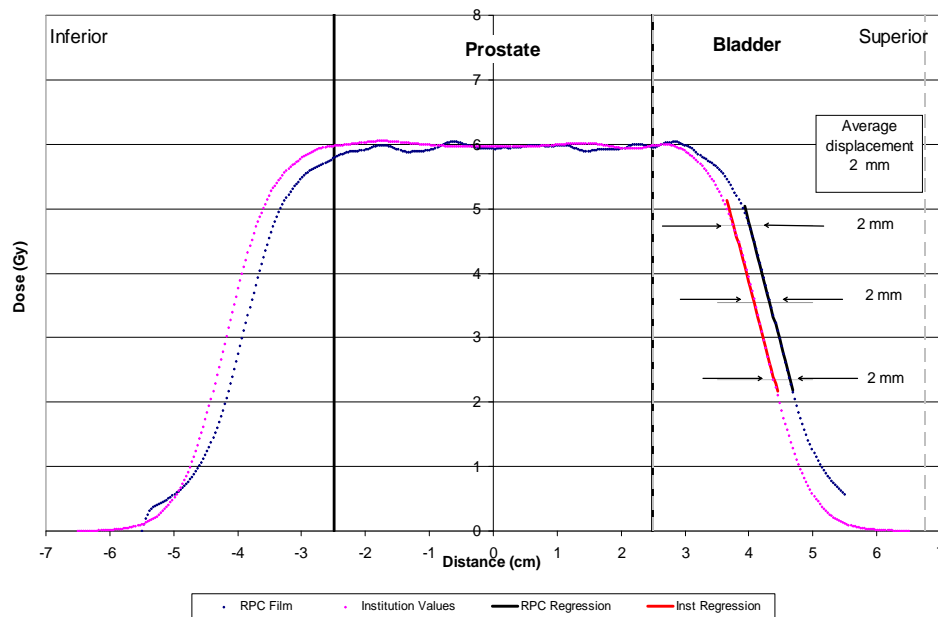


Figure 3.9: Plan 1 Trial 1 Superior-Inferior Profile – Sagittal Plane

The superior-inferior profile was captured on both the coronal and the sagittal films. These are shown in Figure 3.8 and Figure 3.9 respectively. Both displacements are less than 3 mm. Both film profiles appear to be shifted more towards the superior side of the phantom. This can be attributed to a shift in setup. As the phantom was set up using laser markings, a 1 mm setup error is not unlikely.

The lasers at the PTC-H are only calibrated with the gantry at 270° and are not normally used for patient setup. The on-board imaging system is used to localize patients through bony anatomy. When the phantom is on the treatment table, the only anatomy that could be used for localization would be the femur material which are two symmetrical cylinders. The concern that this would not provide the necessary landmarks to adequately position the phantom led to the use of the laser markings from the CT scan.

The registrations of the sagittal films also have a larger registration error than the

coronal films. For the set of films in Plan 1 Trial 1, the root mean square (RMS) of the 2D registration for the coronal film was 0.24 mm while the sagittal film had a RMS of 0.87 mm. This is most likely due to the fact that the sagittal film is cut in two separate pieces yet still registered as one solid piece. The film must be carefully scanned to minimize the registration error. For these reasons, a small difference in the superior-inferior profiles between the two films is accepted.

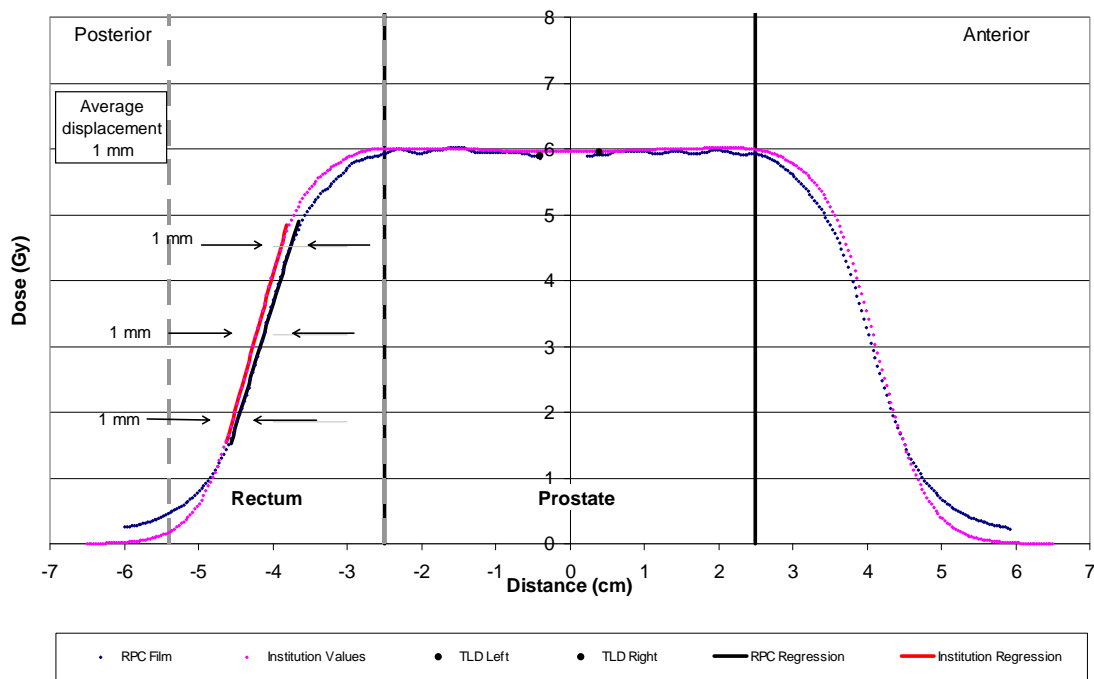


Figure 3.10: Plan 1 Trial 1 Anterior-Posterior Profile – Sagittal Plane

The last profile garnered from the film was the anterior-posterior profile from the sagittal film as seen in Figure 3.10. For this trial, the displacement was 1 mm with good agreement along the entire profile. Note that the center of the film data is missing. This is where the film was cut to intersect with the coronal film. The solid black dots indicate the locations of the TLD. Note that the TLD are placed on either side of the cut in the film.

This enables the film dose of each piece of the sagittal film to be scaled to an absolute dose point.

For Treatment Plan 2, the same profiles were taken to compare the measured and TPS predicted dose to the phantom. From the TLD dose in Section 3.5.1, we expected the film dose to be lower than calculated, but the range of the beam was still expected to follow the plan. In Figure 3.11, this is not what was seen.

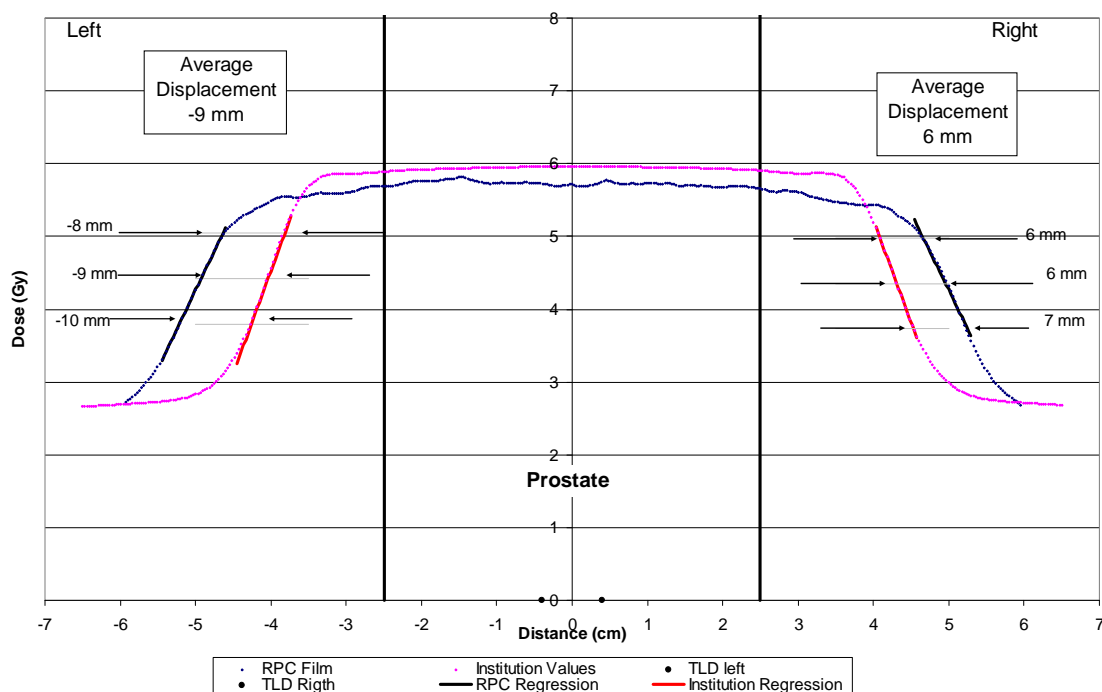


Figure 3.11: Plan 2 Trial 1 Right Left Profile – Coronal Plane

The film dose profile extends well beyond the calculated dose profile on both the right and left sides of the target. The average displacement is -9.0 mm on the left side and 6.0 mm on the right side. This does not portray a shift in the phantom positioning as the result of a setup error would shift the film profile in one direction. The other three film dose profiles (Figure 3.12, Figure 3.13, and Figure 3.14) were all within 3 mm of the TPS

dose profiles. The superior-inferior profiles in Figure 3.12 and Figure 3.13 showed a shift towards the superior edge of the phantom of 3 mm. This is believed to be from a shift in the initial setup of the phantom. The anterior-posterior profile in Figure 3.14 has no shift and is considered a perfect match with 0 mm displacement.

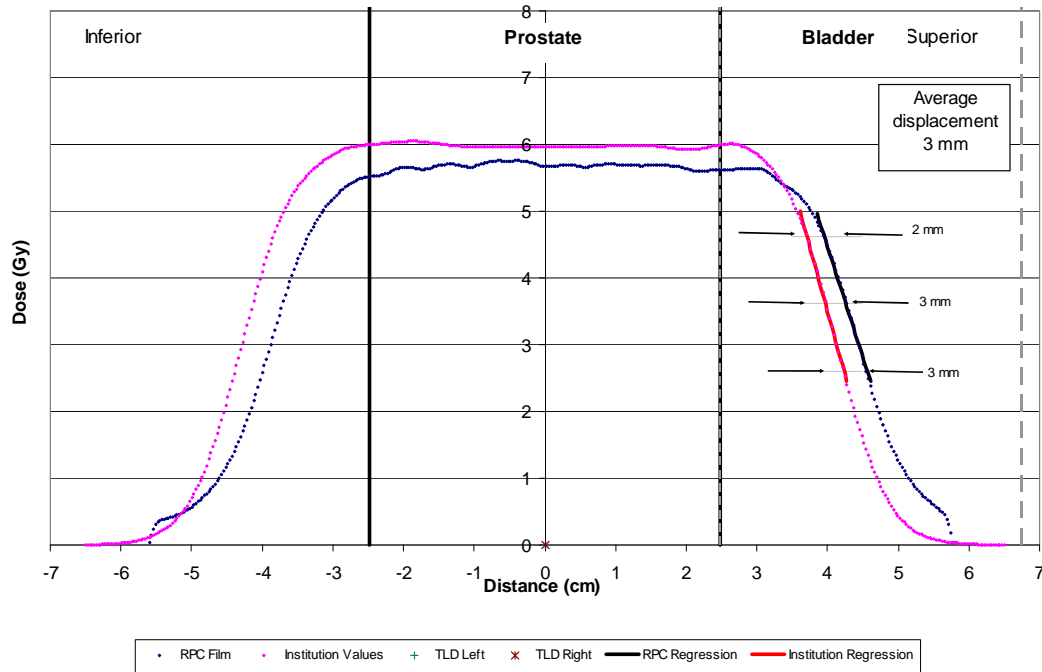


Figure 3.12: Plan 2 Trial 1 Superior-Inferior Profile – Coronal Plane

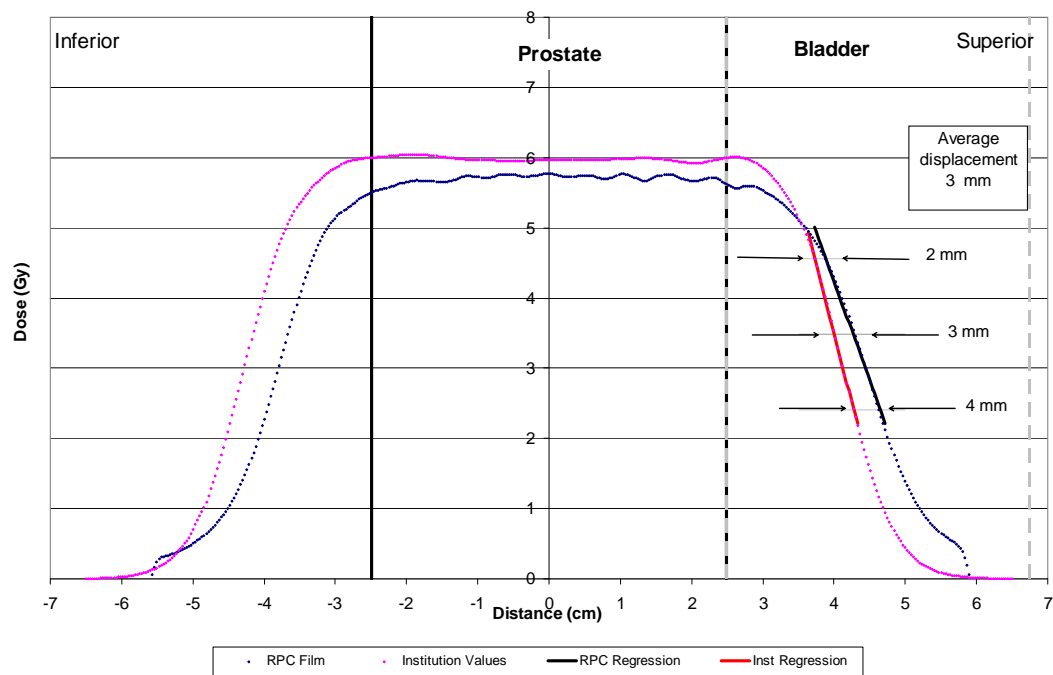


Figure 3.13: Plan 2 Trial 1 Superior-Inferior Profile – Sagittal Plane

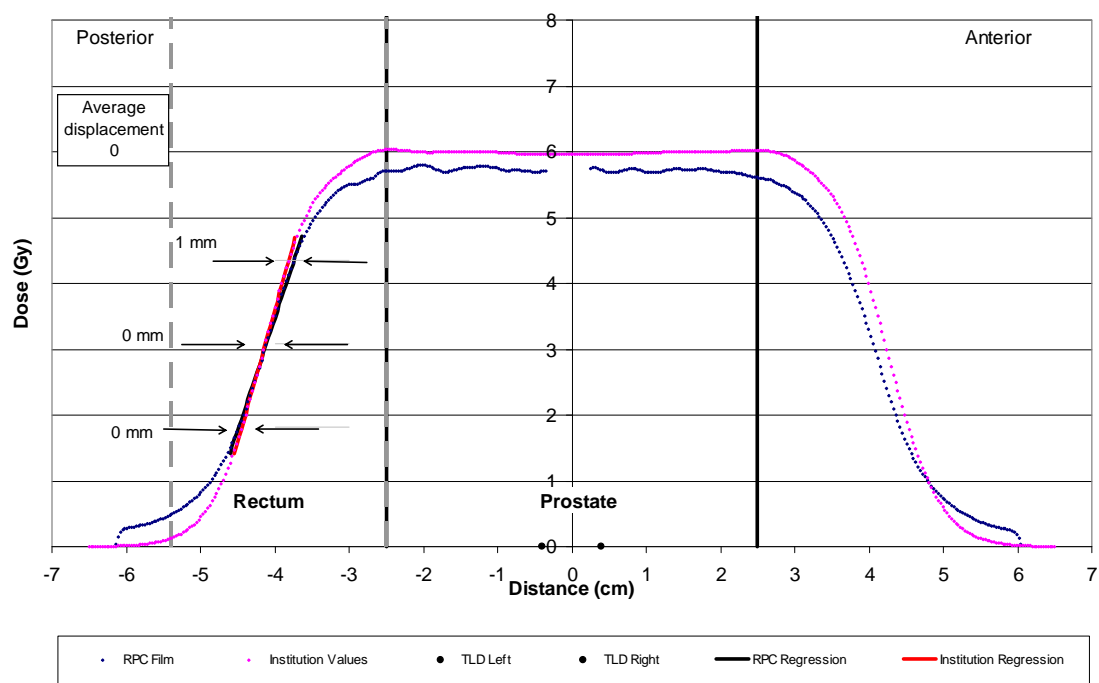


Figure 3.14: Plan 2 Trial 1 Anterior-Posterior Profile – Sagittal Plane

Trials 2 and 3 from Treatment Plan 2 are shown in the Appendix and correspond well with Trial 1. For Trials 1 and 2 there were no failing film profiles outside of the Right-Left profiles. Trial 3 failed on the Superior-Inferior profile in the sagittal plane with a 4 mm displacement.

The film profiles for Plan 2 were also compared to the calculated dose profiles from the dosimetry insert on the verification plan. The relative stopping powers for the dosimetry insert (composed of HI Polystyrene) could have resulted in a measurable difference in the proton range.

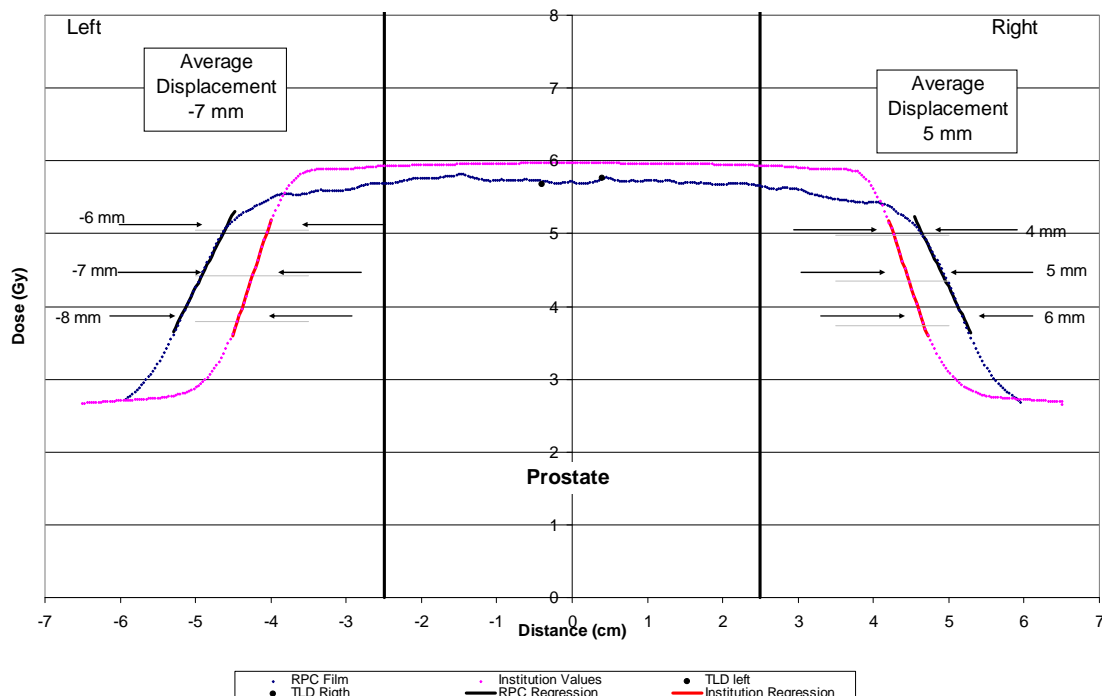


Figure 3.15: Plan 2 Verification Trial 1 Right Left Profile – Coronal Plane

Comparing Figure 3.11 and Figure 3.15, there was an improvement in measured displacement with the beam fluence calculated on the dosimetry insert (versus the imaging insert). The verification plan's margin (Figure 3.15) was still outside of the

accepted limits of 3mm. For trial 1 the average displacement was -7 mm on the left side and 5 mm on the right side. Trials 2 and 3 (listed in the Appendix) also failed the set criteria of 3 mm in the right left direction. The other verification profiles from Plan 2 (Figure 3.16 Figure 3.18) did not change beyond 1 mm in comparison to the Plan 2 profiles in Figure 3.12 -Figure 3.14.

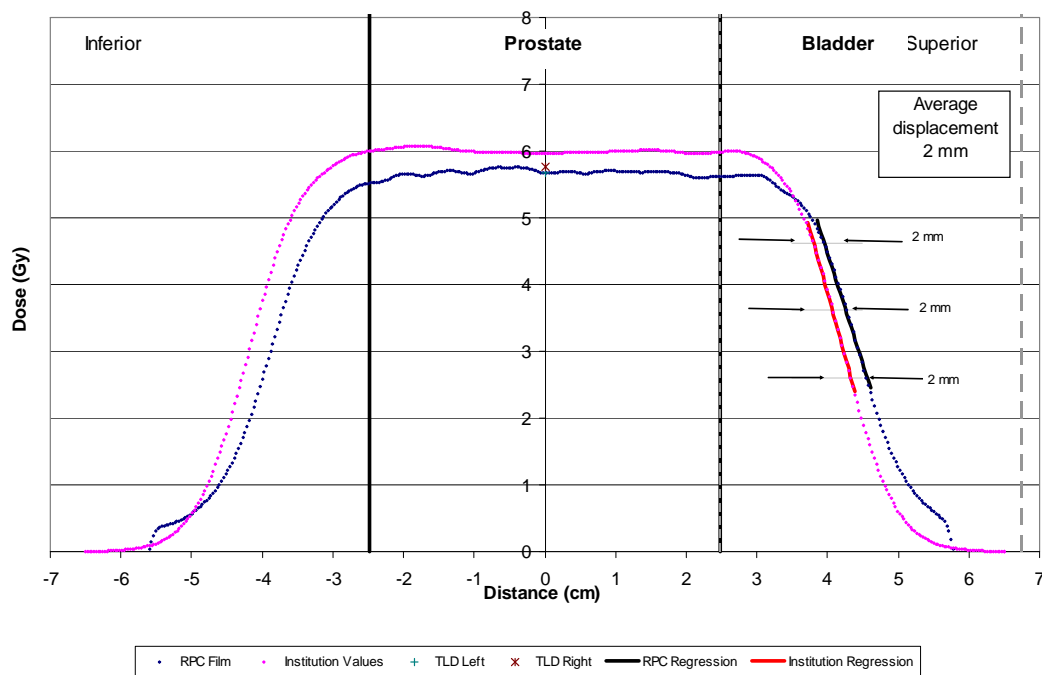


Figure 3.16: Plan 2 Verification Trial 1 Superior-Inferior Profile – Coronal Plane

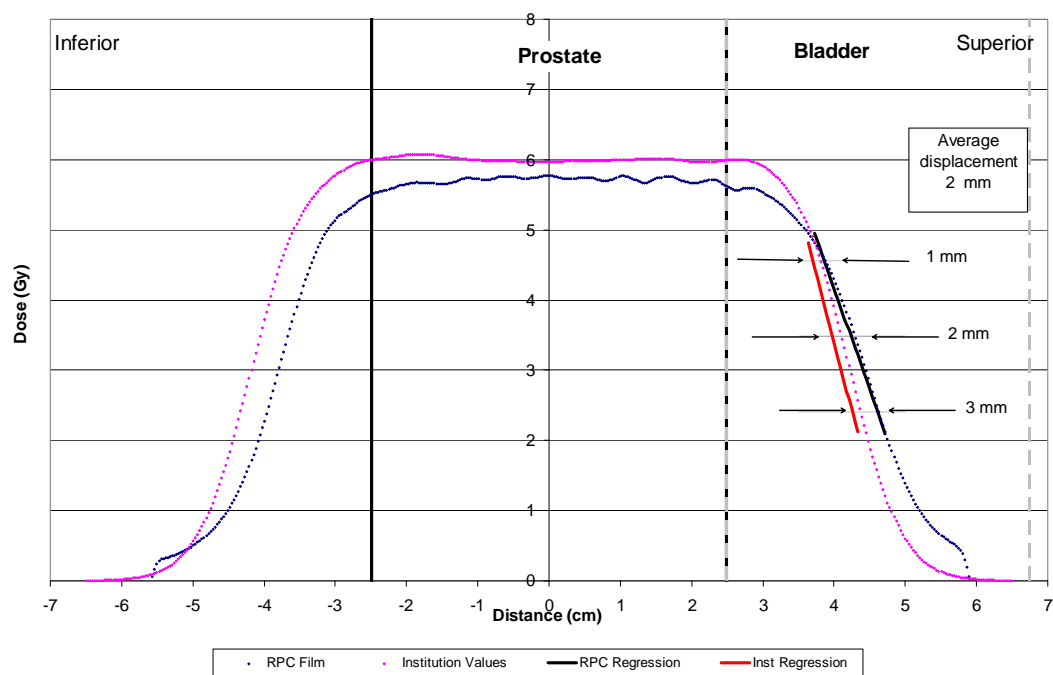


Figure 3.17: Plan 2 Verification Trial 1 Superior-Inferior Profile – Sagittal Plane

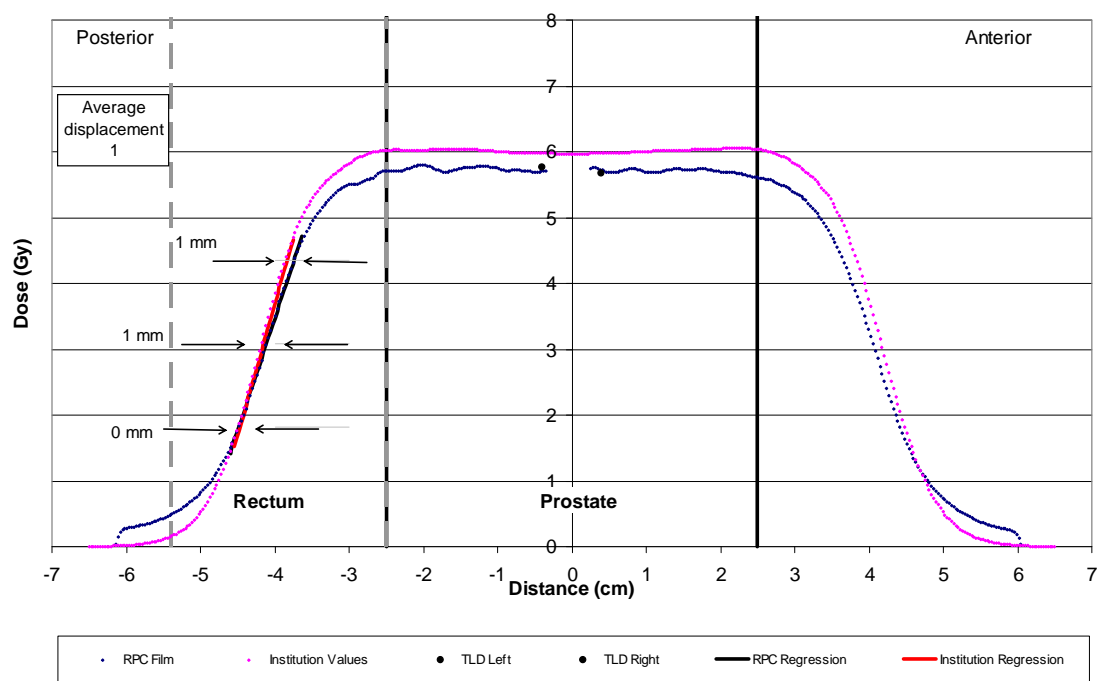


Figure 3.18: Plan 2 Verification Trial 1 Anterior-Posterior Profile – Sagittal Plane

Overall the maximum shift between trials for both treatment plans was 2 mm. For instance, the shift in the anterior-posterior profile for Plan 1 was 1 mm for all 3 trials. For Plan 2 the superior-inferior profile in the sagittal plane was 3 mm for Trials 1 and 2 and 4 mm for Trial 1 giving a 1mm shift between trials. This 2 mm agreement between trials shows the film profiles can be reproduced within our 3 mm margin.

3.5.3 Treatment Plan 2 Quality Assurance

With the large displacement in right-left profile for Treatment Plan 2, it was decided to perform a quality assurance test in the same style that would be done for a patient treatment. This test ensures that the plan calculated by the TPS is being delivered by the machine.

The measured and calculated depth dose profiles were compared to one another and can be seen in Figure 3.19 and Figure 3.20.

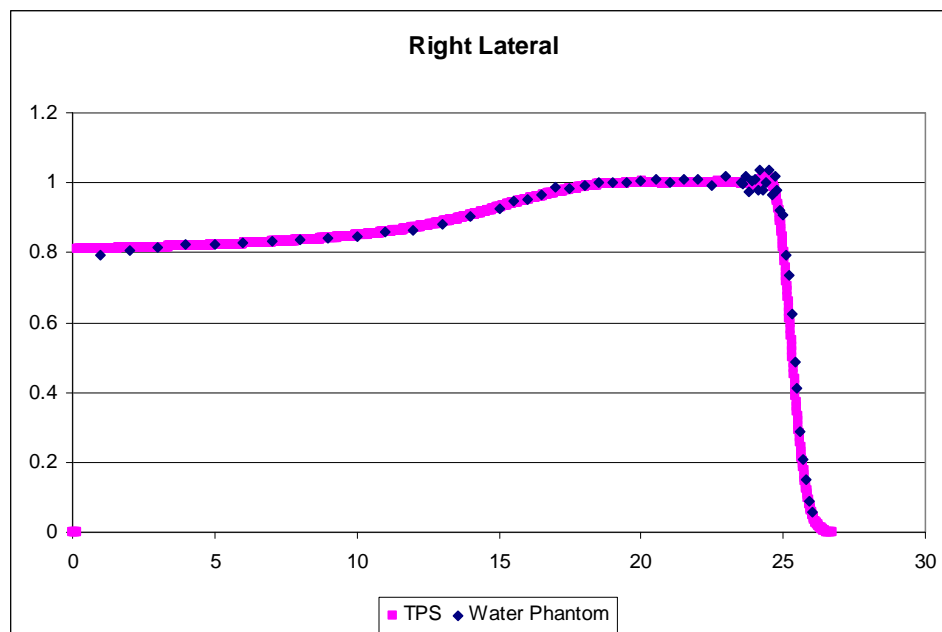


Figure 3.19: Right Lateral QA Comparison

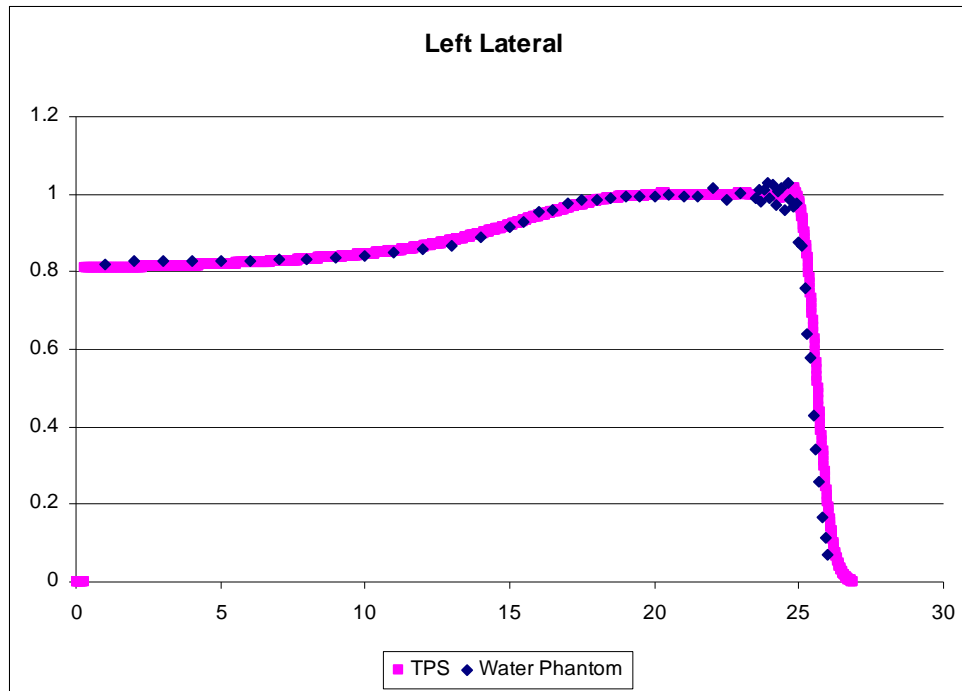


Figure 3.20: Left Lateral QA Comparison

A spline interpolation was performed to calculate the shift of the distal 90% of the measured beam profile and the calculated beam profile. The right lateral scan was shifted by 0.12 cm and the left lateral scan was shifted by 0.23 cm. These displacements were not large enough to account for the shifts seen in Figure 3.11. From this we concluded that the difference in beam profiles most likely is attributed to one of two things:

- The effect of the protons streaming along the film plane and the difference in composition between the HI polystyrene and film itself, or
- An error in measurement of the relative stopping power of the phantom materials and subsequent entry into the TPS

By rotating the dosimetry insert 10°, the film would no longer be parallel to the beam and any streaming effects would be negated. Air gaps had already been eliminated by double-loading the film in the dosimetry insert.

The material stopping power measurements were only done once for each material. Though the comparison of the measured stopping powers and published literature values agreed within 5%, this difference could have been the source of the range differences. The range of the beam could have penetrated further than expected on both the left and right side of the target due to a discrepancy between the measured stopping powers and the actual stopping powers of the material. This suggests the stopping powers used in calculating Treatment Plan 2 were larger than the actual stopping power encountered by the protons. The new stopping powers input into the TPS were mainly increasing the assigned stopping power initially produced by the calibration curve from HU to relative SP. Given the chance, scanning the materials several times with different material widths might produce a more accurate relative stopping power.

Chapter 4

Conclusions

4.1 Summary

This research was intended to evaluate the Radiological Physics Center's pelvis phantom for use in auditing proton therapy treatment procedures. The guidelines set for a passing score were to have no more than a 5%/3mm difference between the measured dose and the calculated dose with a reproducibility of 3%.

The first part of the project involved measuring the relative stopping powers of the materials used to construct the phantom. As the phantom was originally designed to evaluate photon IMRT procedures, the materials chosen were not necessarily proton-equivalent. By using samples of the different materials in the pelvis phantom, the relative stopping powers were measured and plotted along with CT values assigned to the materials. Comparing the measured values to the HU-SP calibration curve used by the TPS, it was found that the stopping powers for the materials could be underestimated by 5-10%. With this knowledge, the phantom was tested under two main conditions:

- Using the patient calibration curve already in place by the TPS
- Overriding the calibration curve to use material specific stopping powers

The phantom was simulated and planned using the clinic procedures in place for a typical prostate treatment. Once the plan was approved, the dose to the target was scaled to deliver 6 Gy. The phantom was irradiated 3 separate times using Plan 1. All of the measured planned target volume (PTV) TLD values for Plan 1 were well within 5% of the calculated dose from the TPS. The COV for the PTV doses were both less than 0.4% while the COV for the femoral head doses were less than 0.7%. For Plan 1, all of the

trials for all 4 profiles showed a displacement that was less than 3 mm.

The CT numbers were then overridden on the treatment plan to account for the actual stopping powers of the materials as previously measured. The beams were re-calculated and the phantom was irradiated 3 separate times using Plan 2. The measured dose from Plan 2 was on average 3% lower than its counterparts in Plan 1. Two of the TLD measurements (PTV Left in trials 1 and 2) differed more than 5% from the calculated measurements. These did not pass the set criteria of 5%/3mm. By placing the beams to the dosimetry insert, all of the measured dose points came within the 5% range of the calculated dose. The right-left film dose profile extended well beyond the calculated dose profile on both the right and left sides of the target. The average displacement was -9.0 mm on the left side and 6.0 mm on the right side. For Trials 1 and 2 there were no failing film profiles outside of the Right-Left profiles. Trial 3 failed on the Superior-Inferior profile in the sagittal plane with a 4 mm displacement.

With the large displacements encountered with Plan 2, several measures were taken to confirm the results. The beams were placed on a “verification plan” which re-calculated the beams based on the dosimetry insert instead of the imaging insert. This changed the displacements in the left-right direction. The verification plan’s margin was still outside of the accepted limits of 3mm. For trial 1 the average displacement was -7 mm on the left side and 5 mm on the right side.

4.2 Conclusions

The hypothesis of this work was to use the pelvis phantom to confirm agreement between the measured and calculated dose within 5%/3mm with a reproducibility of 3%.

Plan 1 passed the established criteria and the results indicted the phantom would be an acceptable tool for auditing proton therapy. With the phantom materials not being considered proton-equivalent materials, any institution that did not pass an audit involving the pelvis phantom could cite the phantom composition as a contributing factor to any discrepancies in dose margins. A solution to the difference in Hounsfield units and relative stopping powers of the materials was to directly input the measured stopping powers into the treatment planning system for dose calculation as was done for Plan 2.

Plan 2 was intended to improve the agreements and instead introduced large displacements along the path of the beam. More work will have to be performed to find the source of the displacements. Plan 2 more closely represents the actual phantom composition (as compared to Plan 1 which did not use the corrected stopping powers) and should easily pass the set criteria of an agreement between the measured dose and calculated dose within 5%/3mm. At this time, the hypothesis was proven incorrect and the current version of the pelvis phantom was determined not suitable to evaluate proton therapy treatment procedures. With only one film profile failing the requirement, further studies could resolve the current issues and the phantom will be better suited for remote auditing of proton therapy treatment procedures.

4.3 Future works

The pelvis phantom shows promise as a valuable tool in the remote auditing proton therapy. One instance of future work on this phantom is to rotate the film in the phantom so the film is placed at an angle to the beam. This would remove any effect from the protons traveling along the film plane and having a change in density between the

dosimetry insert and the film.

Many of the Gafchromic© film studies in the literature are from MD-55 film. An updated set of measurements for Gafchromic© EBT and EBT2 film in proton beams could be done to confirm previous findings have not been negated by an update in the film.

As the pelvis phantom represents simple anatomy, and therefore a relatively simple treatment plan, once this phantom has been commissioned for use with protons, other relevant anatomical locations should also be tested. With more complicated treatment plans, the phantom's ability to accurately measure the dose delivered to a target would become more imperative in order to audit procedures in the corresponding treatment sites.

Chapter 5

Appendix

The following figures are the additional the film profiles from trials 2 and 3 of each irradiation referred to in Section 3.5.2.

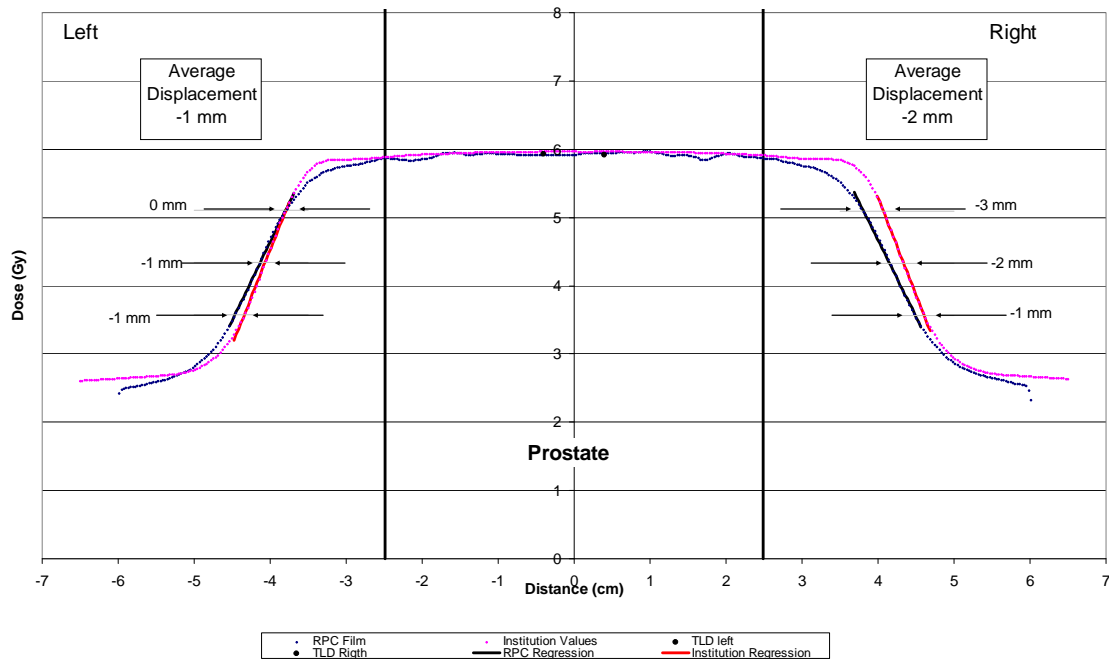


Figure 5.1: Plan 1 Trial 2 Right-Left Profile – Coronal Plane

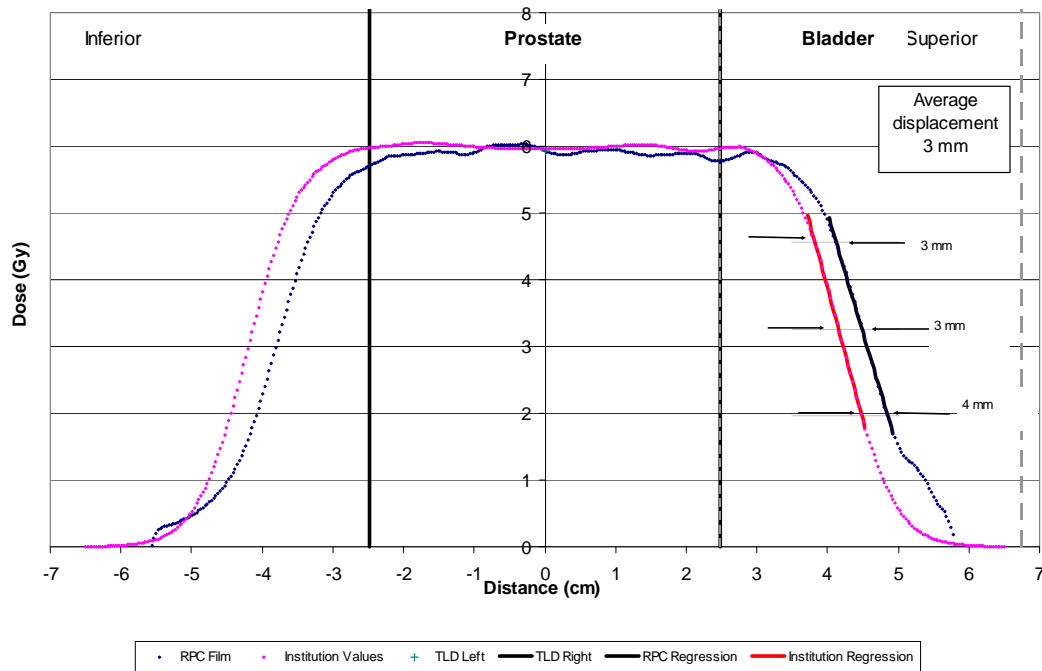


Figure 5.2: Plan 1 Trial 2 Superior-Inferior Profile – Coronal Plane

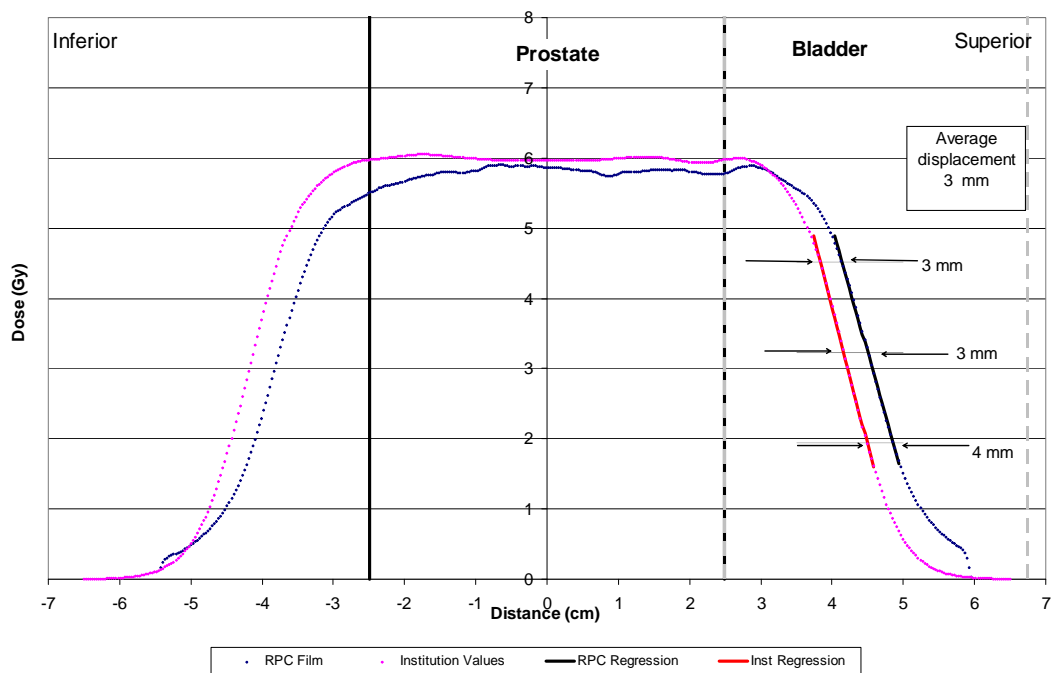


Figure 5.3: Plan 1 Trial 2 Superior-Inferior Profile – Sagittal Plane

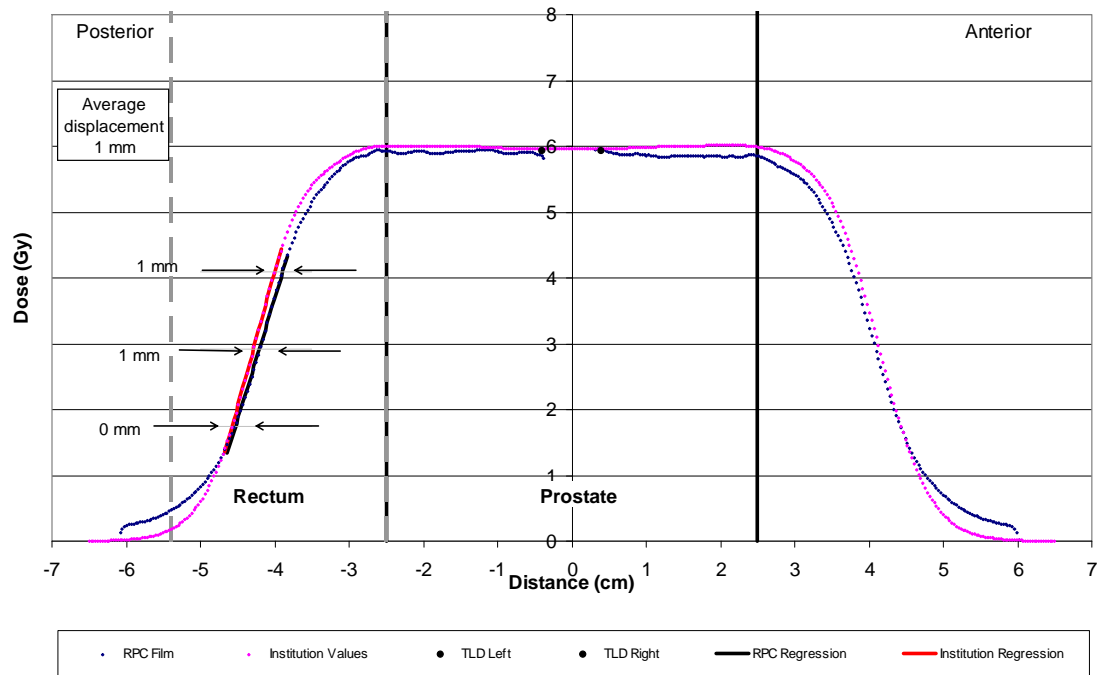


Figure 5.4: Plan 1 Trial 2 Anterior-Posterior Profile – Sagittal Plane

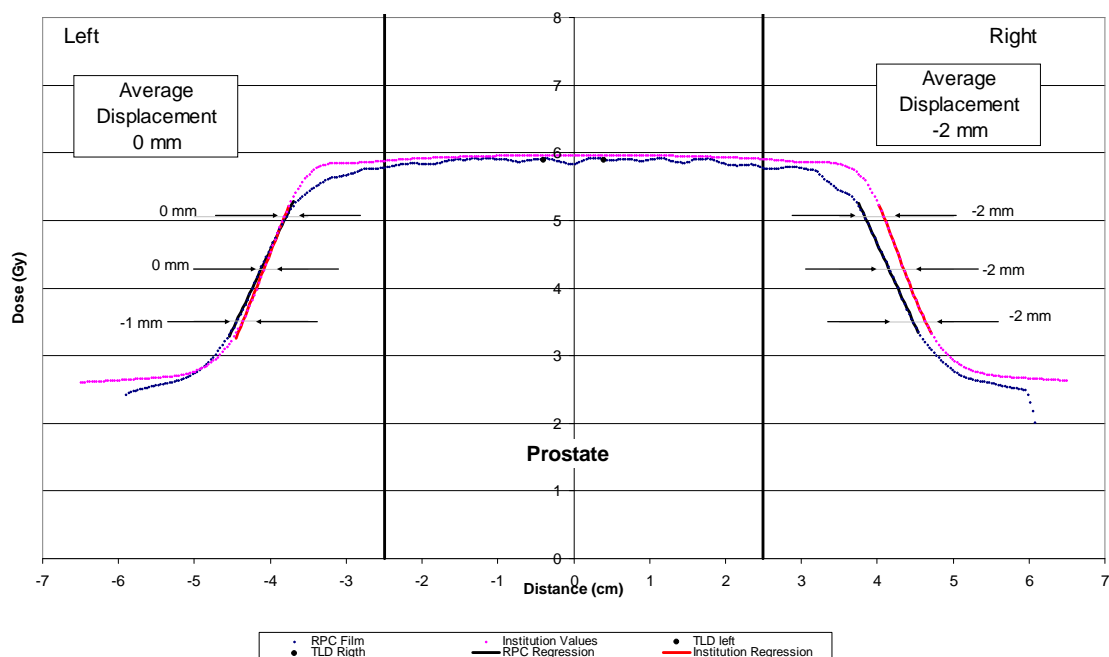


Figure 5.5: Plan 1 Trial 3 Right-Left Profile – Coronal Plane

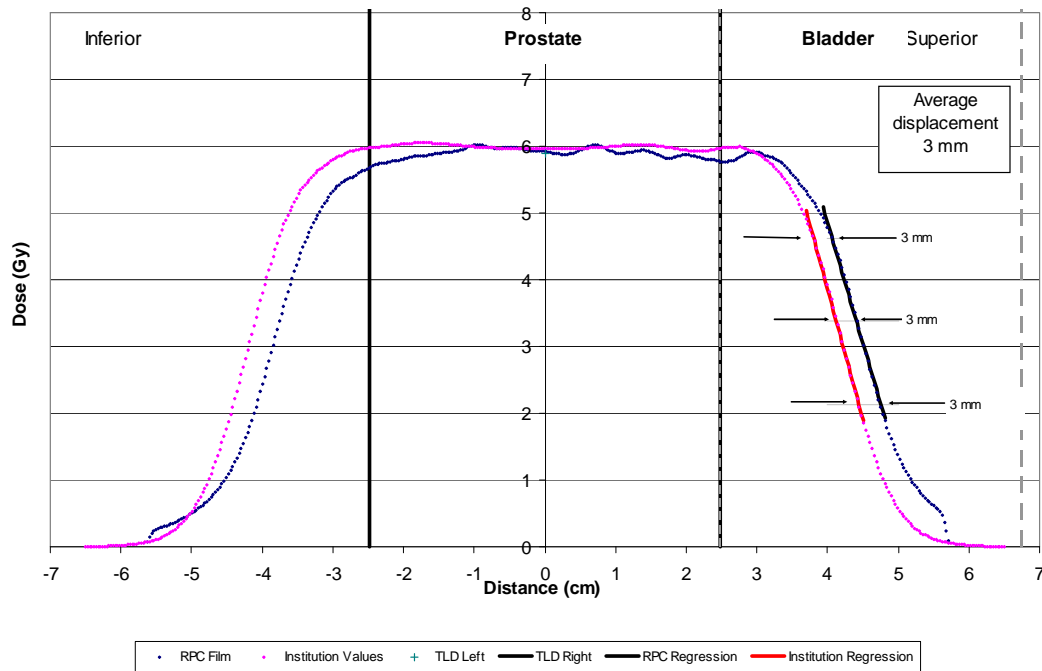


Figure 5.6: Plan 1 Trial 3 Superior-Inferior Profile – Coronal Plane

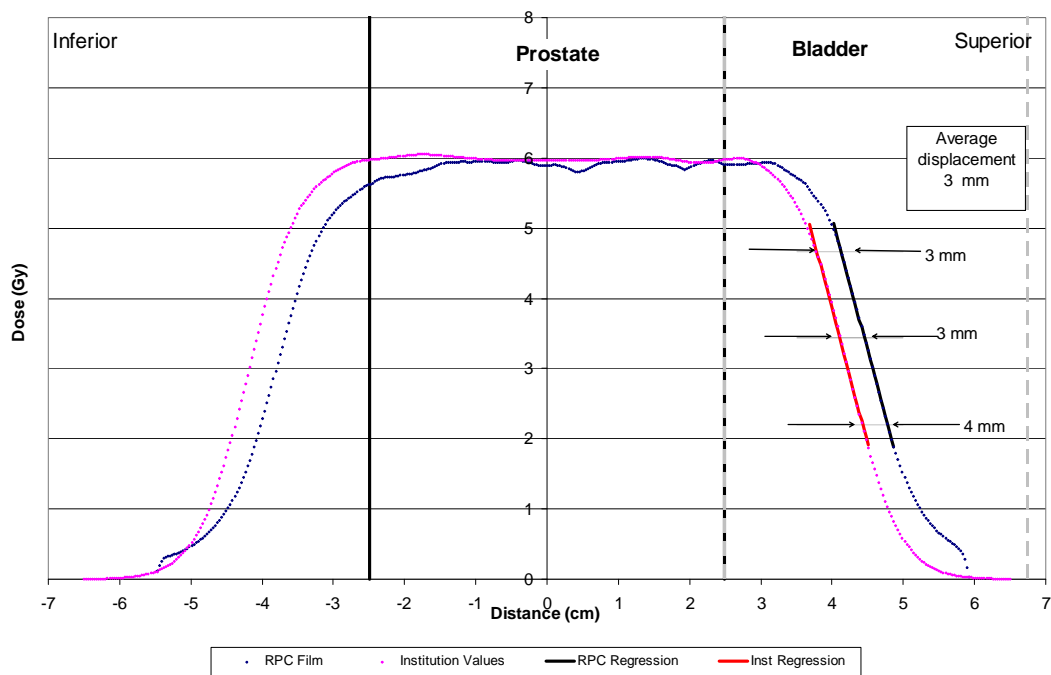


Figure 5.7: Plan 1 Trial 3 Superior-Inferior Profile – Sagittal Plane

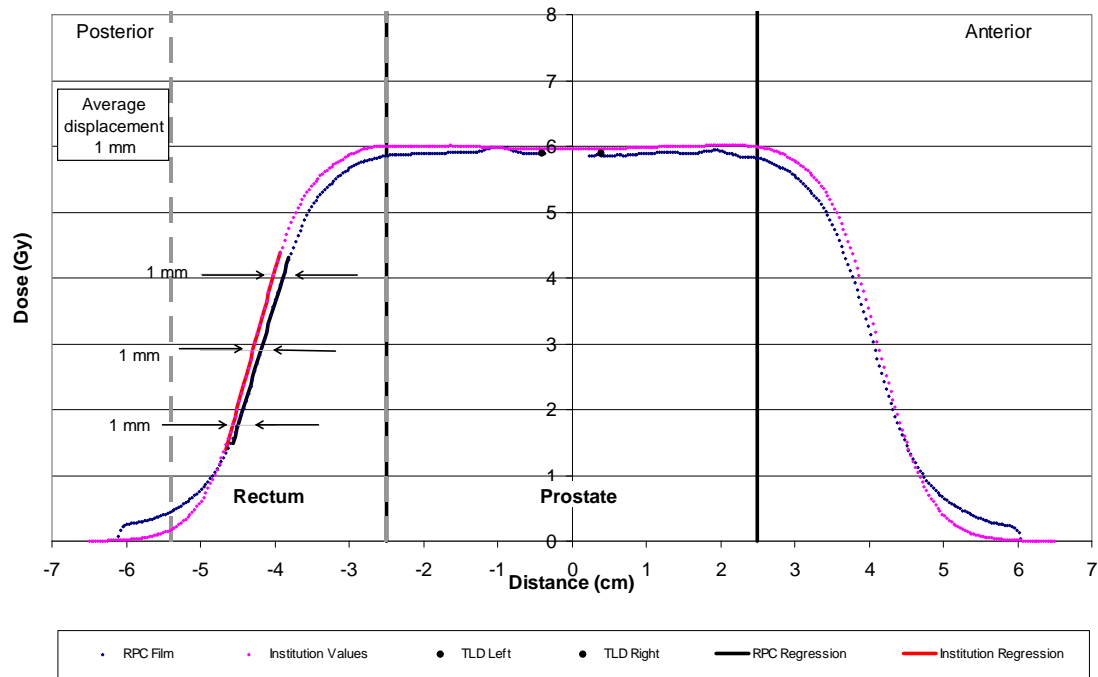


Figure 5.8: Plan 1 Trial 3 Anterior-Posterior Profile – Sagittal Plane

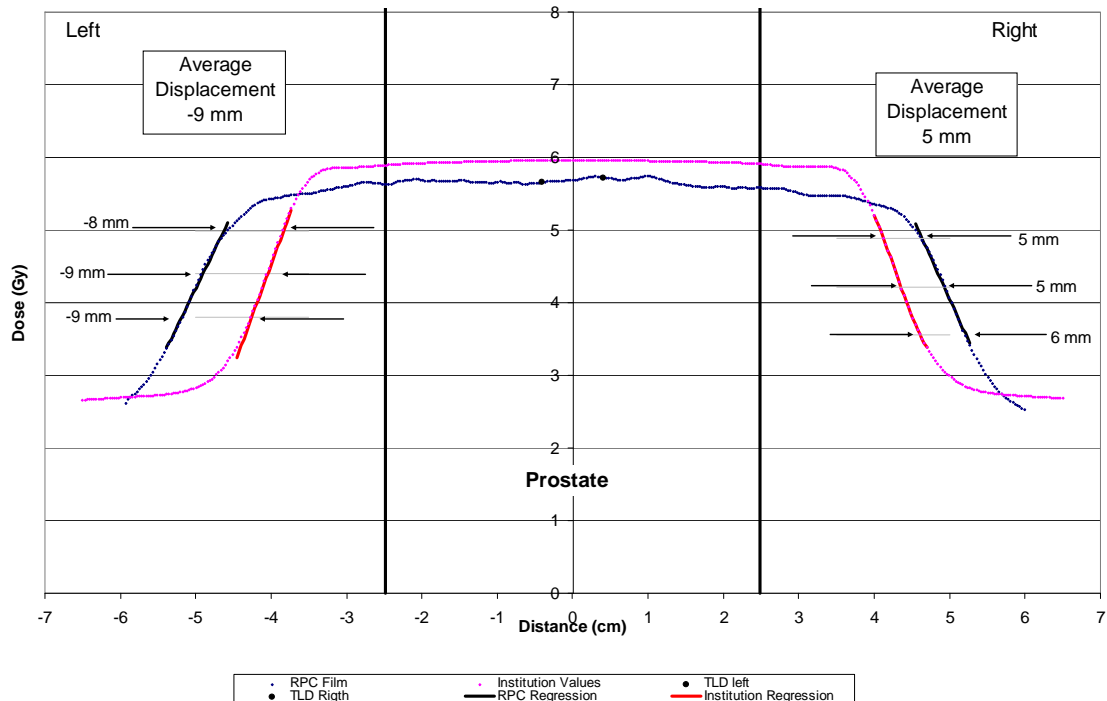


Figure 5.9: Plan 2 Trial 2 Right Left Profile – Coronal Plane

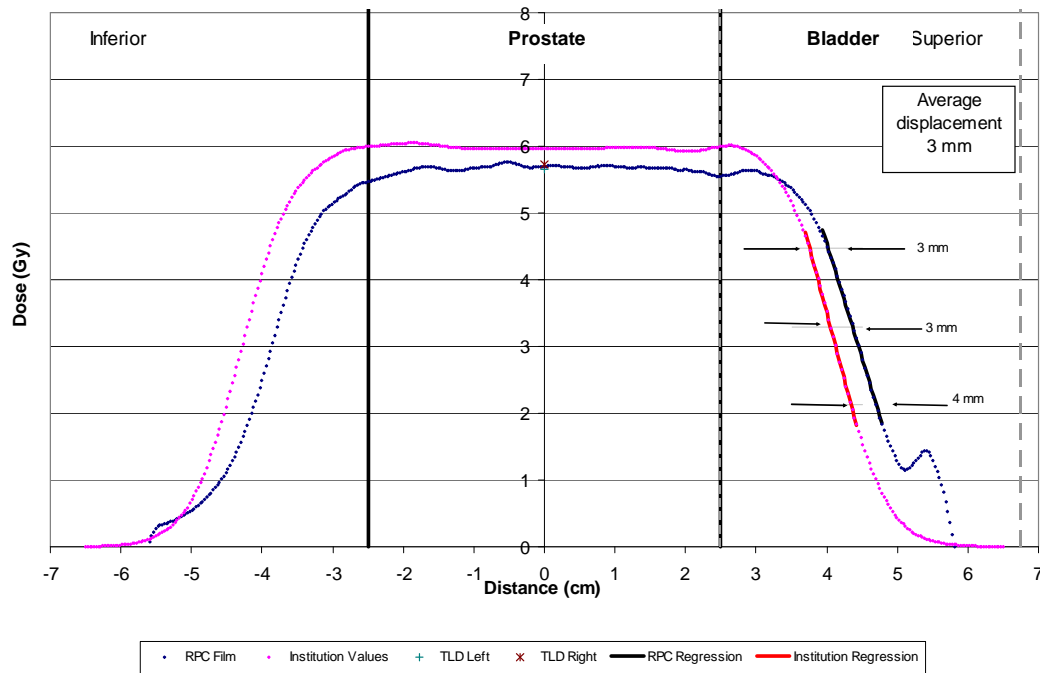


Figure 5.10: Plan 2 Trial 2 Superior-Inferior Profile – Coronal Plane

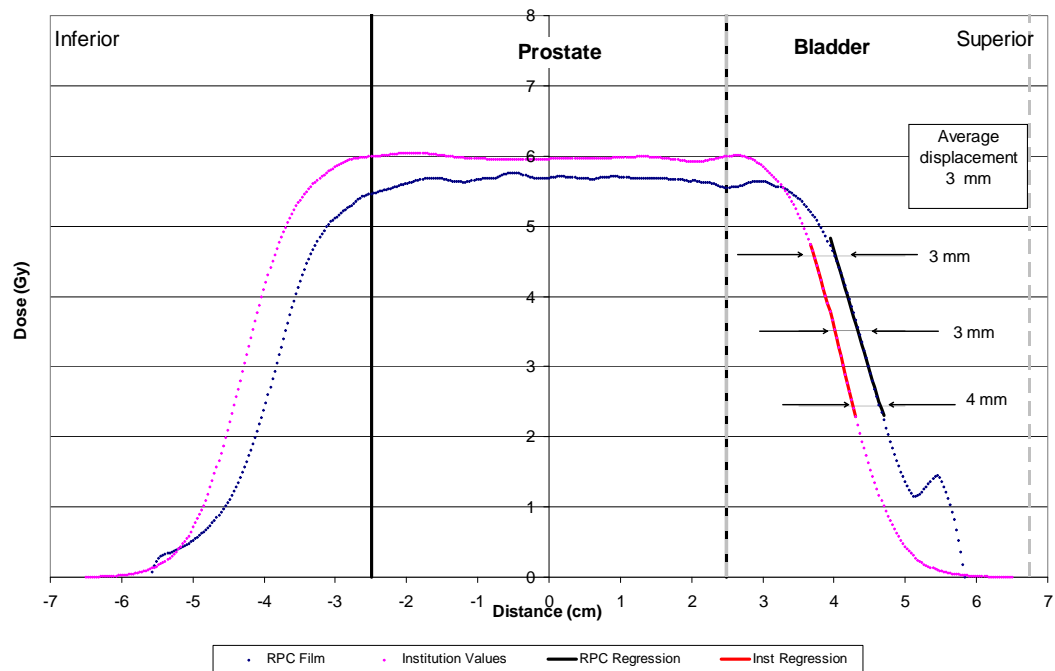


Figure 5.11: Plan 2 Trial 2 Superior-Inferior Profile – Sagittal Plane

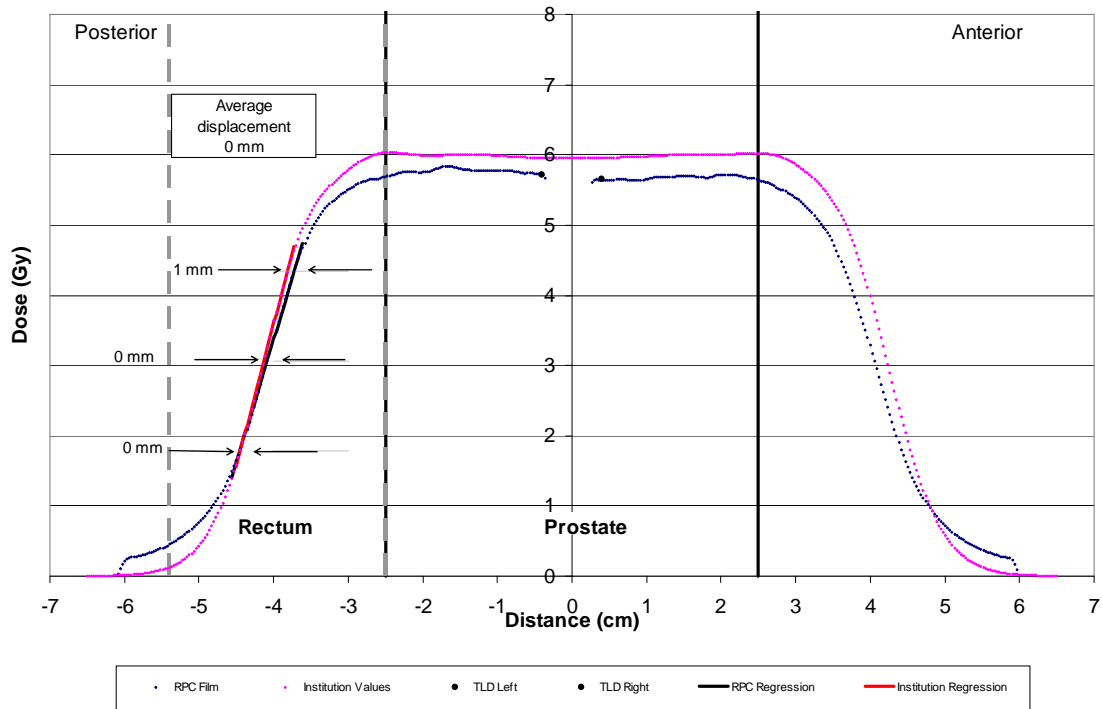


Figure 5.12: Plan 2 Trial 2 Anterior-Posterior Profile – Sagittal Plane

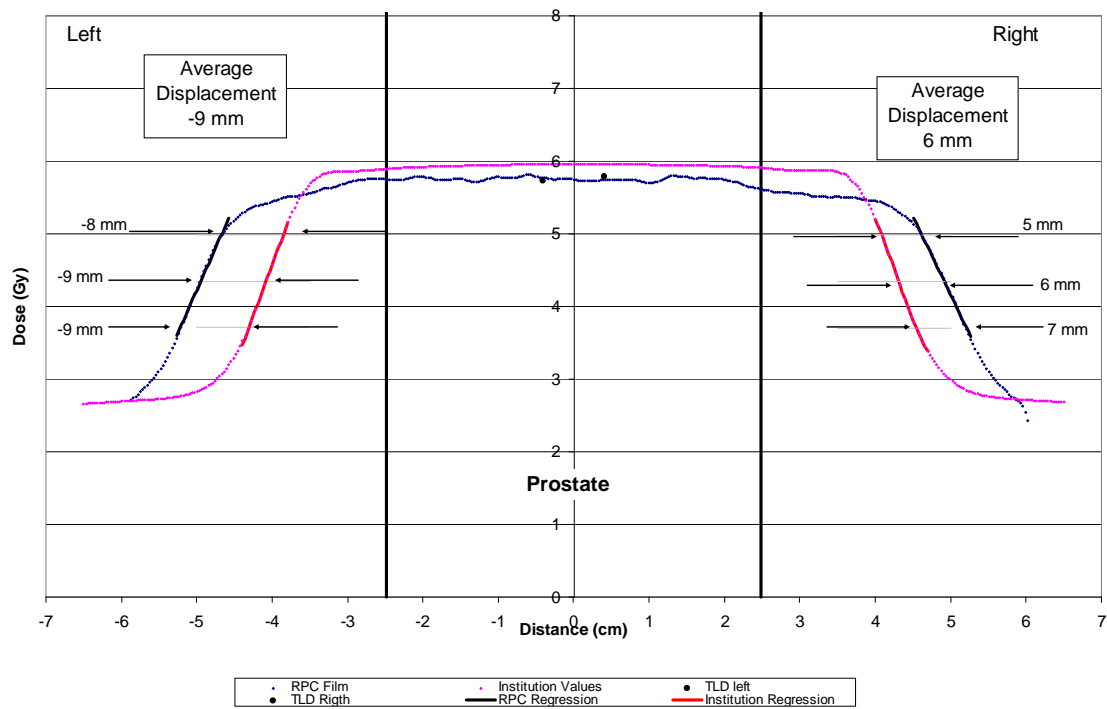


Figure 5.13: Plan 2 Trial 3 Right Left Profile – Coronal Plane

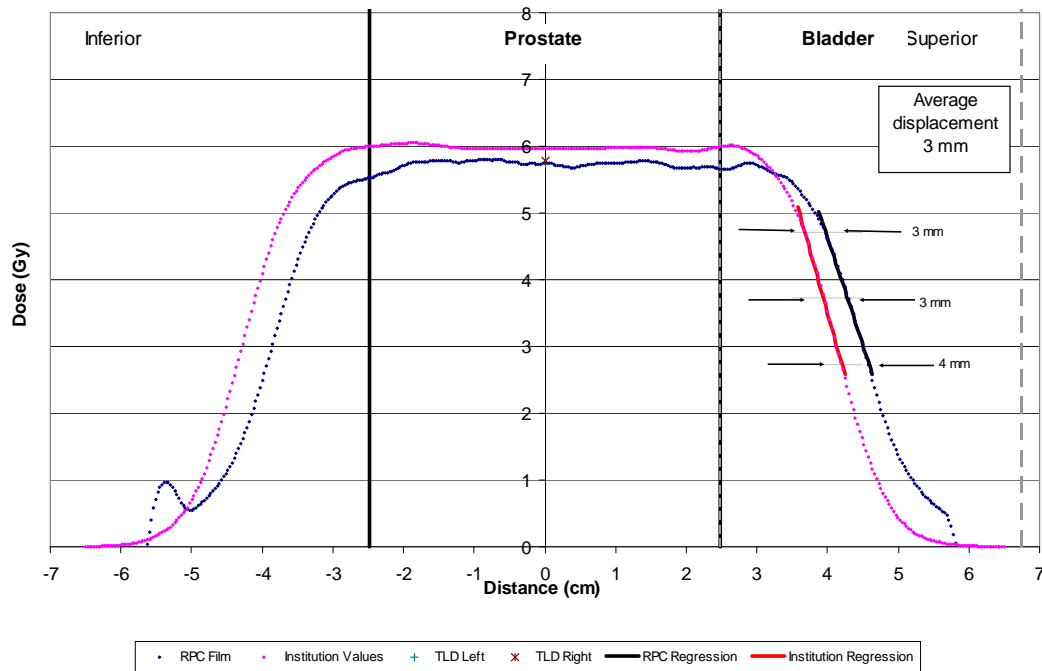


Figure 5.14: Plan 2 Trial 3 Superior-Inferior Profile – Coronal Plane

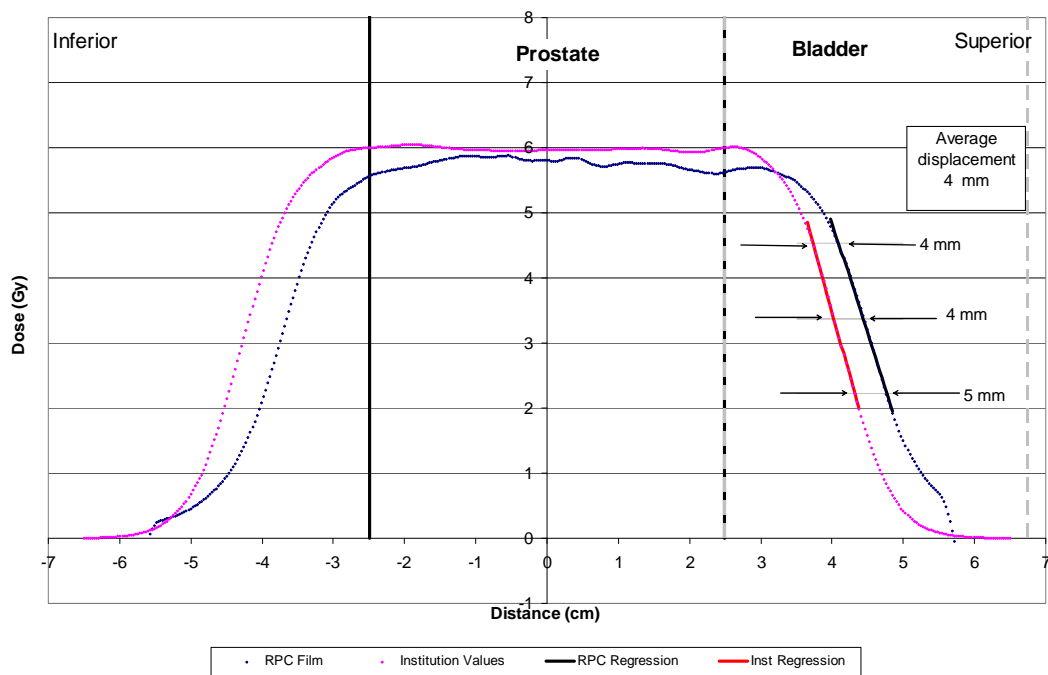


Figure 5.15: Plan 2 Trial 3 Superior-Inferior Profile – Sagittal Plane

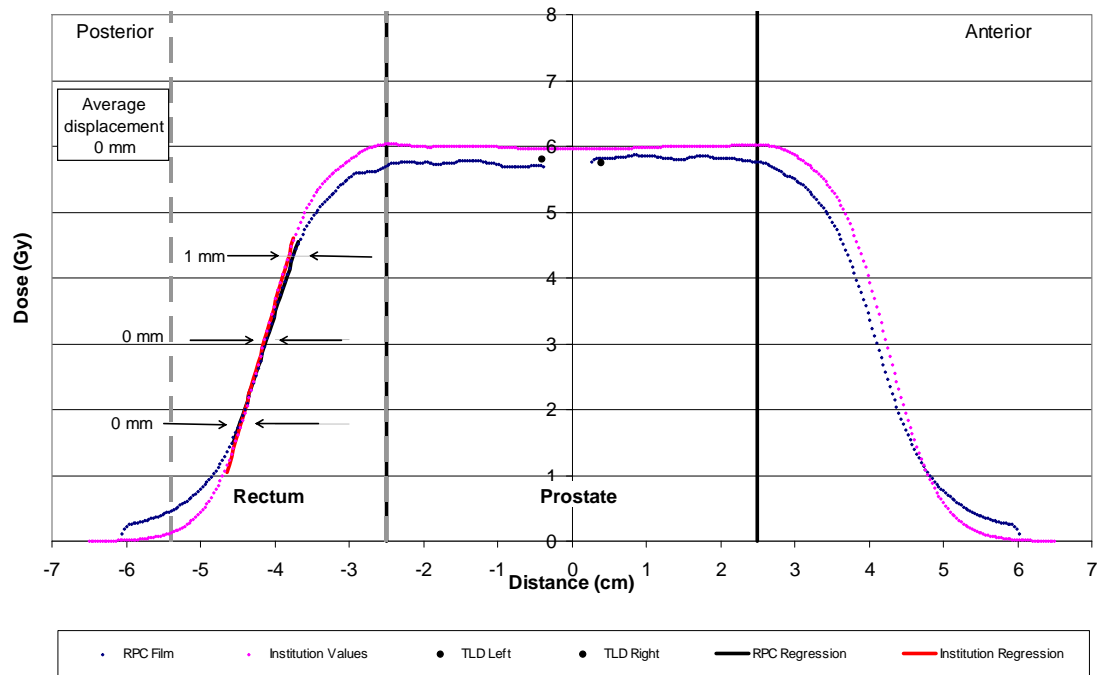


Figure 5.16: Plan 2 Trial 3 Anterior-Posterior Profile – Sagittal Plane

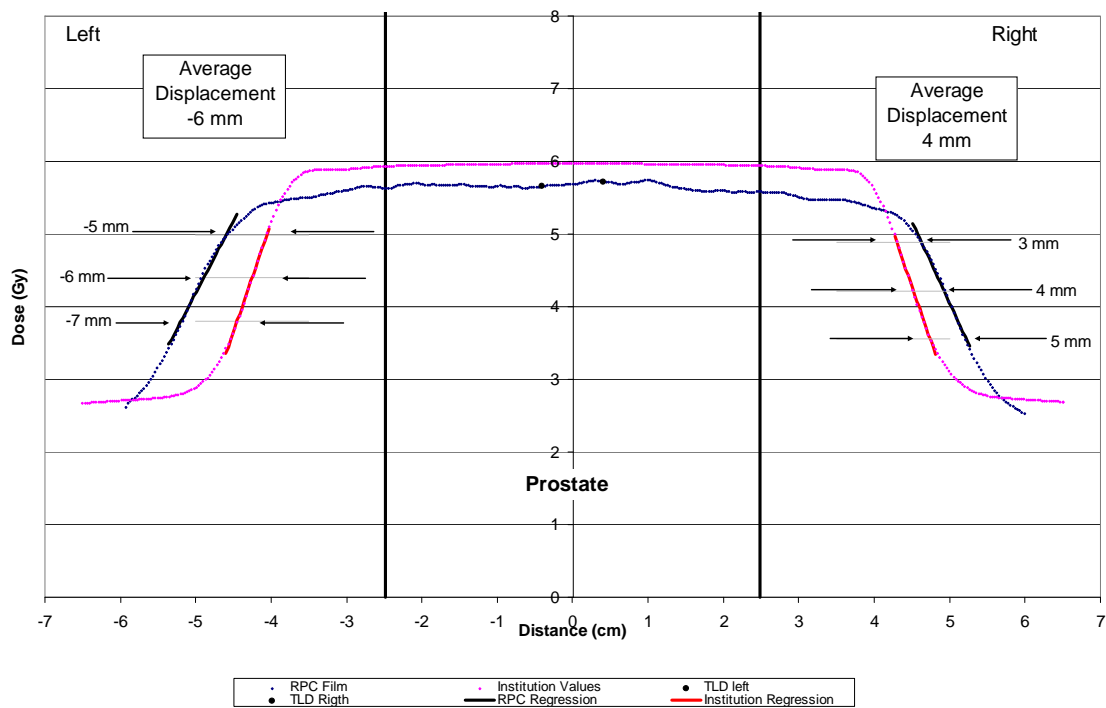


Figure 5.17: Plan 2 Verification Trial 2 Right Left Profile – Coronal Plane

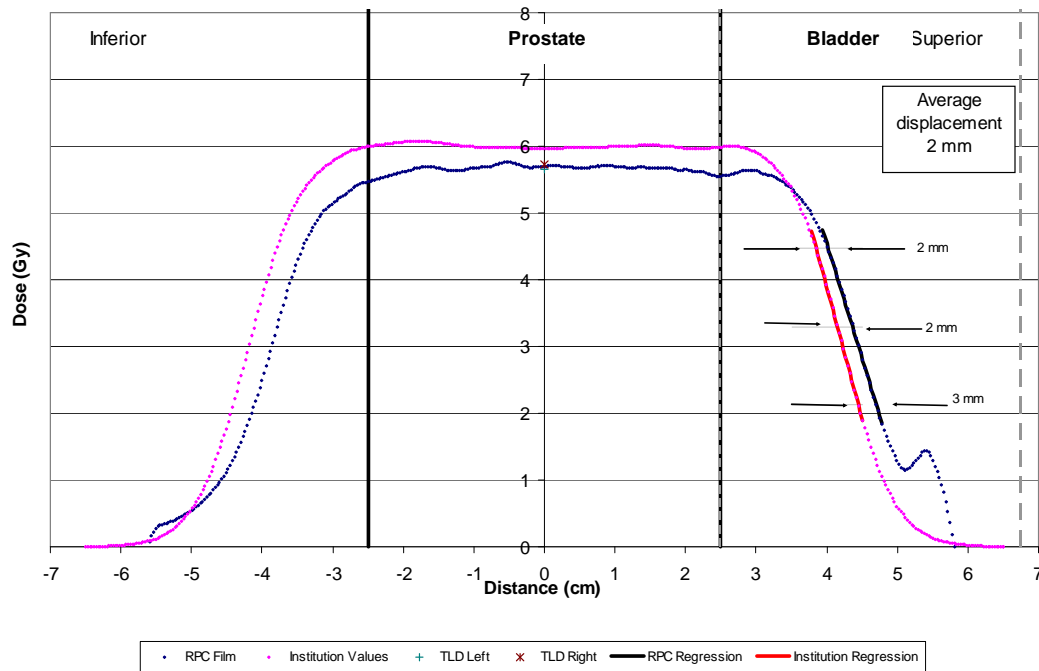


Figure 5.18: Plan 2 Verification Trial 2 Superior-Inferior Profile – Coronal Plane

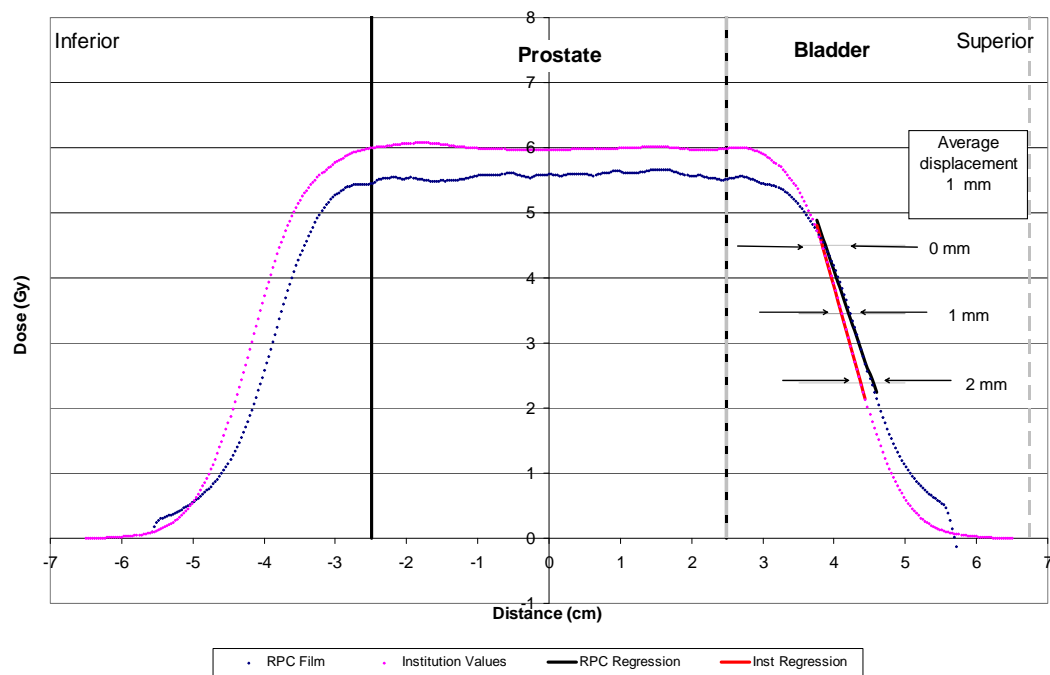


Figure 5.19: Plan 2 Verification Trial 2 Superior-Inferior Profile – Sagittal Plane

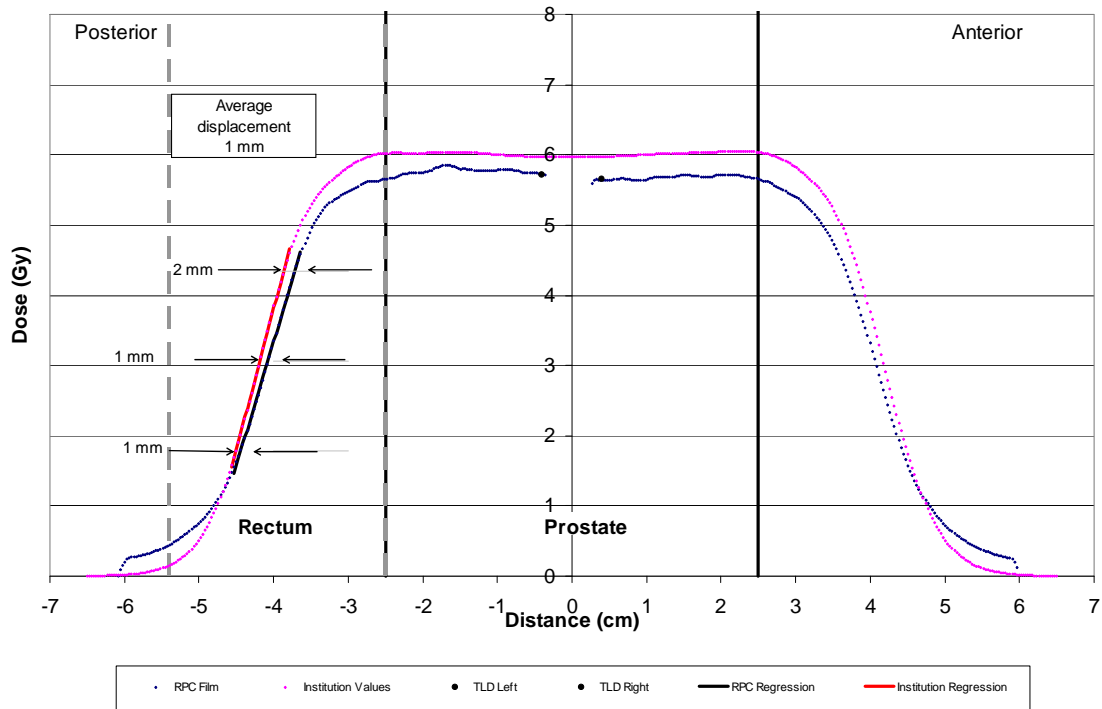


Figure 5.20: Plan 2 Verification Trial 2 Anterior-Posterior Profile – Sagittal Plane

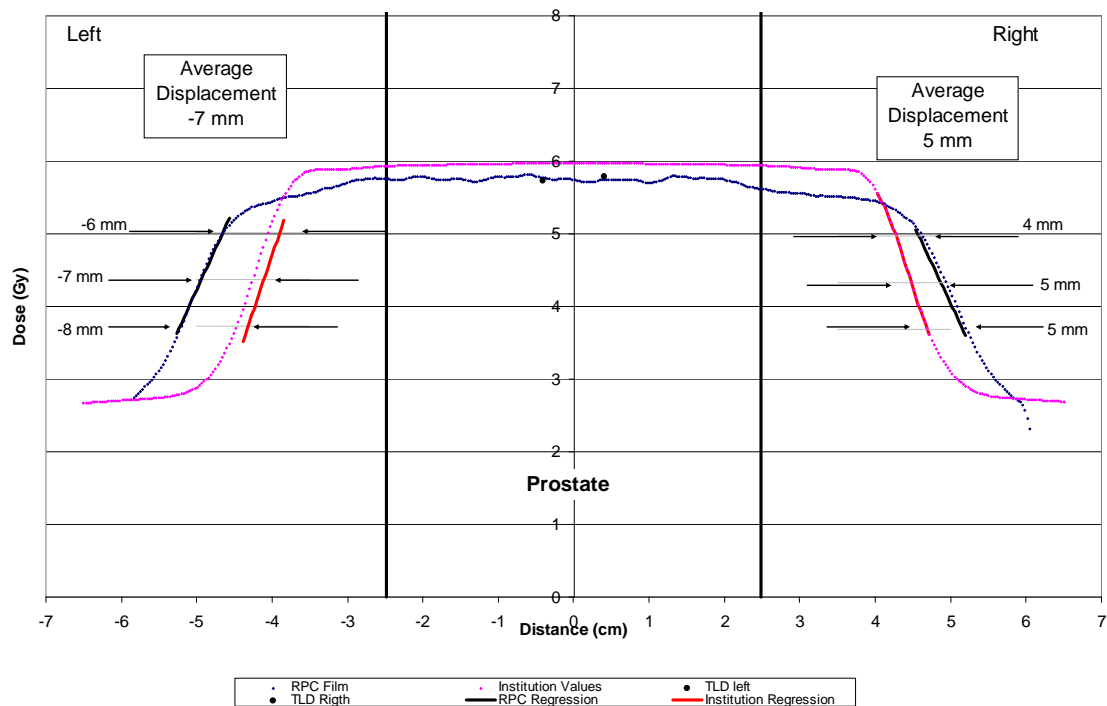


Figure 5.21: Plan 2 Verification Trial 3 Right Left Profile – Coronal Plane

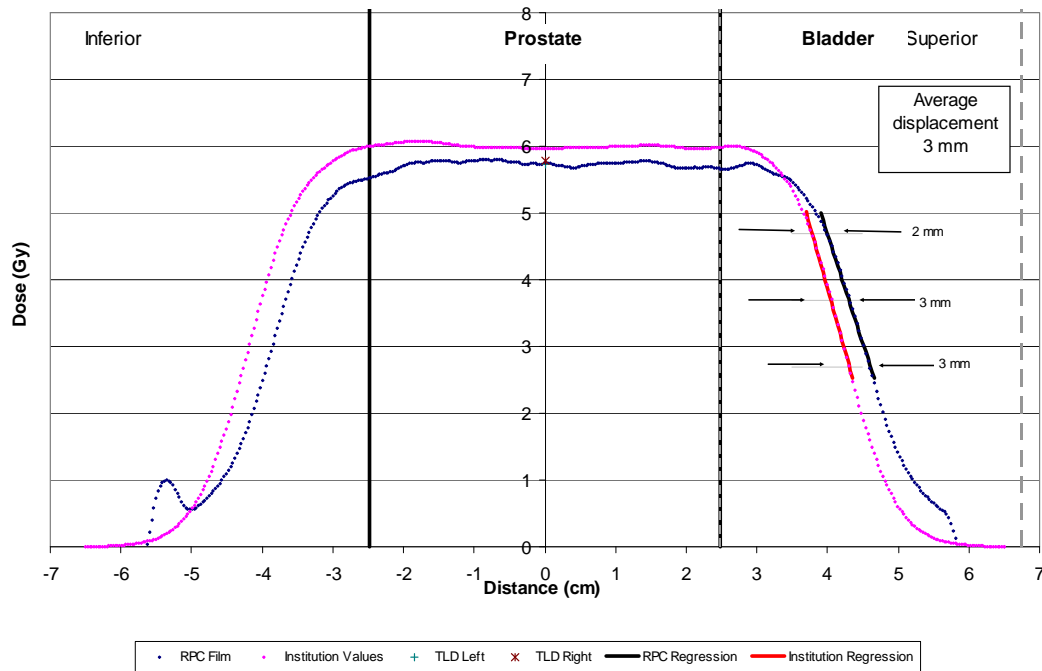


Figure 5.22: Plan 2 Verification Trial 3 Superior-Inferior Profile – Coronal Plane

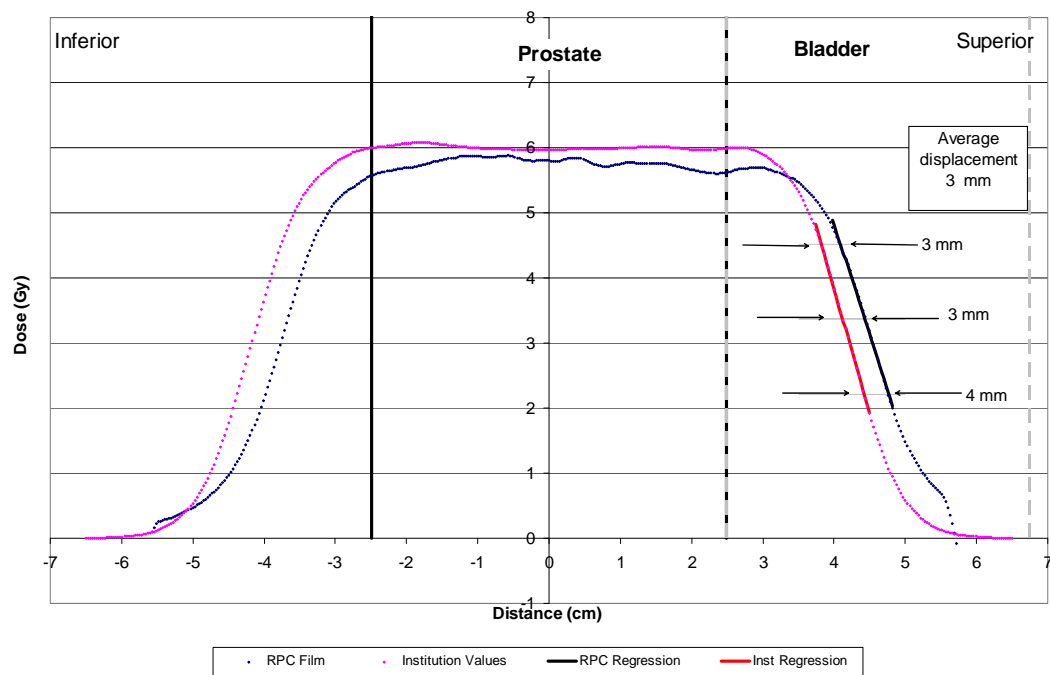


Figure 5.23: Plan 2 Verification Trial 3 Superior-Inferior Profile – Sagittal Plane

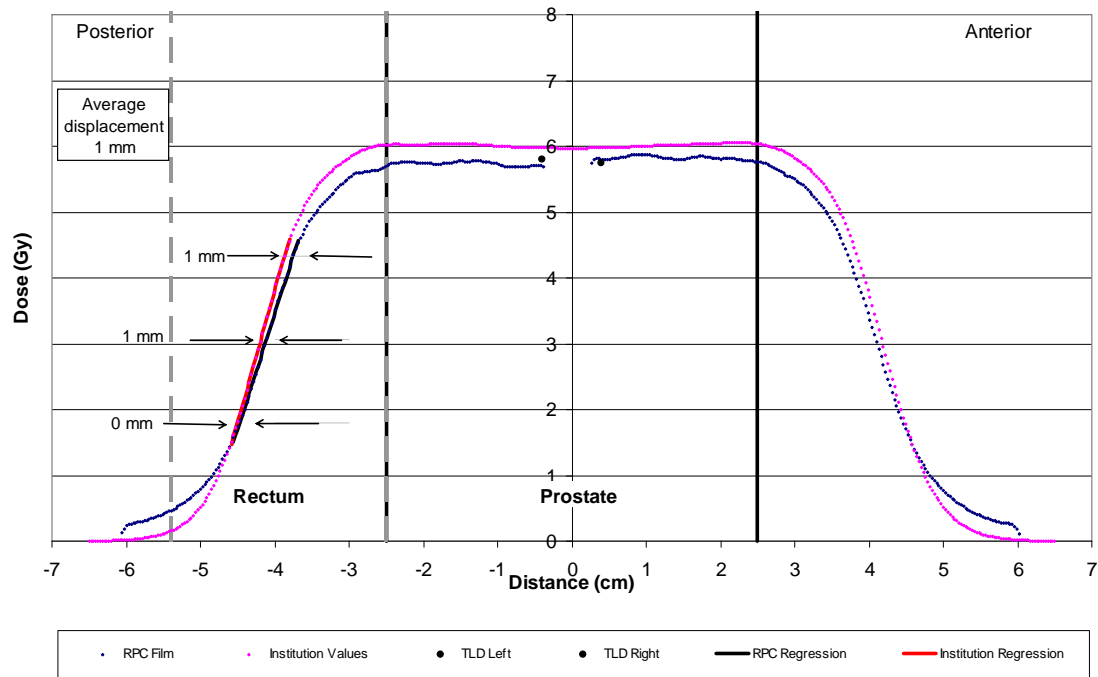


Figure 5.24: Plan 2 Verification Trial 3 Anterior-Posterior Profile – Sagittal Plane

References

- Andreo, P., Burns, D. T., Hohlfeld, K., Huq, M. S., Kanai, T., Laitano, F., Smyth, V. and Vynckier, S. (2000). "Absorbed dose determination in external beam radiotherapy: An international code of practice for dosimetry based on standards of absorbed dose to water." IAEA Technical report series No. 398.
- Breuer, H. and Smit, B. J. (2000). Proton therapy and radiosurgery. Berlin ; New York, Springer.
- Deasy, J. O., Blanco, A. I. and Clark, V. H. (2003). "CERR: a computational environment for radiotherapy research." Med Phys **30**(5): 979-85.
- Followill, D. S., Evans, D. R., Cherry, C., Molineu, A., Fisher, G., Hanson, W. F. and Ibbott, G. S. (2007). "Design, development, and implementation of the radiological physics center's pelvis and thorax anthropomorphic quality assurance phantoms." Med Phys **34**(6): 2070-6.
- ICRU (1993). Stopping Power and Ranges for Protons and Alpha Particles. ICRU Report 49. Bethesda, MD.
- ICRU (2007). "Prescribing, Recording, and Reporting Proton-Beam Therapy." Journal of the ICRU **7**(2).
- ISP (2007). Gafchromic EBT Self-Developing Film for Radiotherapy Dosimetry. White Paper, ISP.
- Johns, H. E. and Cunningham, J. R. (1983). The physics of radiology. Springfield, Ill., Thomas.
- Kirby, T. H., Hanson, W. F. and Johnston, D. A. (1992). "Uncertainty analysis of absorbed dose calculations from thermoluminescence dosimeters." Med Phys

19(6): 1427-33.

Kjellberg, R. N., Sweet, W. H., Preston, W. M. and Koehler, A. M. (1962). "The Bragg peak of a proton beam in intracranial therapy of tumors." Trans Am Neurol Assoc **87**: 216-8.

Knoll, G. F. (2000). Radiation detection and measurement / Glenn F. Knoll. New York, John Wiley & Sons.

Koehler, A. M., Schneider, R. J. and Sisterson, J. M. (1975). "Range Modulators for Protons and Heavy Ions." Nuclear Instruments and Methods **131(3)**: 437-440.

Lawrence, J. H. (1957). "Proton irradiation of the pituitary." Cancer **10(4)**: 795-8.

Moyers, M. (1999). Proton Therapy. Modern Technology of Radiation Oncology: A Compendium for Medical Physicists and Radiation Oncologists. J. V. Dyk. Madison, WI, Medical Physics Publications.

Nerbun, C. (2005). Analysis of MD-55-2 Gafchromic Film as a Dosimetry Ausit System for Proton Therapy. Graduate School of Biomedical Sciences, The University of Texas Health Science Center at Houston. **MS Thesis**.

Radford, D. (2001). A Standardized Method of Quality Assurance for Intensity Modulated Radiation Therapy of the Prostate. Graduate School of Biomedical Sciences, The University of Texas Health Science Center at Houston. **MS Thesis**.

Rasband, W. S. (1997-2009). ImageJ. Bethesda, Maryland, National Institutes of Health.

Rosner, B. (2006). Fundamentals of biostatistics. Belmont, CA, Thomson-Brooks/Cole.

Sahoo, N., Zhu, X. R., Arjomandy, B., Ciangaru, G., Lii, M., Amos, R., Wu, R. and Gillin, M. T. (2008). "A procedure for calculation of monitor units for passively scattered proton radiotherapy beams." Med Phys **35(11)**: 5088-97.

- Schaffner, B. and Pedroni, E. (1998). "The precision of proton range calculations in proton radiotherapy treatment planning: experimental verification of the relation between CT-HU and proton stopping power." Phys Med Biol **43**(6): 1579-92.
- Schneider, U., Pedroni, E. and Lomax, A. (1996). "The calibration of CT Hounsfield units for radiotherapy treatment planning." Phys Med Biol **41**(1): 111-24.
- Slater, J. M., Archambeau, J. O., Miller, D. W., Notarus, M. I., Preston, W. and Slater, J. D. (1992). "The proton treatment center at Loma Linda University Medical Center: rationale for and description of its development." Int J Radiat Oncol Biol Phys **22**(2): 383-9.
- Smith, A. R. (2006). "Proton therapy." Phys Med Biol **51**(13): R491-504.
- Smith, A. R. (2009). "Vision 20/20: proton therapy." Med Phys **36**(2): 556-68.
- Tobias, C. A., Lawrence, J. H., Born, J. L., Mc, C. R., Roberts, J. E., Anger, H. O., Low-Beer, B. V. and Huggins, C. B. (1958). "Pituitary irradiation with high-energy proton beams: a preliminary report." Cancer Res **18**(2): 121-34.
- Vatnitsky, S. M. (1997). "Radiochromic film dosimetry for clinical proton beams." Appl Radiat Isot **48**(5): 643-51.
- Wilson, R. R. (1946). "Radiological Use of Fast Protons." Radiology **47**: 487-191.

Vita

Ryan Leigh Grant was born in St. Petersburg, Florida on April 3, 1985, the daughter of Walter and Caren Grant. After completing her high school education at Bellaire Senior High School in Bellaire, Texas in 2003, she entered The University of Texas at Austin in Austin, Texas. In May 2007, she graduated from The University of Texas at Austin and received the degree of Bachelor of Science with a major in Physics. In August of 2007, she entered the University of Texas Health Science Center at Houston Graduate School of Biomedical Sciences.

Permanent address:

5212 Braeburn
Bellaire, TX 77401